

**RECONSTRUCTION TECHNIQUES IN PARALLEL MAGNETIC RESONANCE
IMAGING**

A Thesis Presented

By

Haitham Mohamed Ahmed Ahmed

To

Faculty of Engineering

Of

Cairo University

In Partial Fulfillment of the Requirements
For the Degree of Doctor of Philosophy
Specializing in Systems and Biomedical Engineering

June, 2010

**RECONSTRUCTION TECHNIQUES IN PARALLEL MAGNETIC RESONANCE
IMAGING**

By

Haitham Mohamed Ahmed Ahmed

A thesis Submitted to the
Faculty of Engineering at Cairo University

In Partial Fulfillment of the
Requirement for the Degree of
DOCTOR OF PHILOSOPHY

In

SYSTEM AND BIOMEDICAL ENGINEERING

Under the supervision of

Prof. Dr. Abou-Bakr M. Youssef
Biomedical Engineering department
Faculty of Engineering
Cairo University

Prof. Dr. Yasser M. Kadah
Biomedical Engineering department
Faculty of Engineering
Cairo University

FACULTY OF ENGINEERING, CAIRO UNIVERSITY

GIZA, EGYPT

June 2010

RECONSTRUCTION TECHNIQUES IN PARALLEL MAGNETIC RESONANCE
IMAGING

By

Haitham Mohamed Ahmed Ahmed

A thesis Submitted to the
Faculty of Engineering at Cairo University
In Partial Fulfillment of the
Requirement for the Degree of
DOCTOR OF PHILOSOPHY

In

SYSTEM AND BIOMEDICAL ENGINEERING

Approved by

Examining Committee

Prof. Dr. Abou-Bakr M. Youssef

Thesis Main Advisor

Prof. Dr. Yasser M. Kadah

Thesis Main Advisor

Prof. Dr. A. Sayed Ahmed

Examiner

Prof. Dr. Fatma El-Hefnawi

Examiner

FACULTY OF ENGINEERING, CAIRO UNIVERSITY
GIZA, EGYPT
June 2010

ABSTRACT

Magnetic resonance imaging (MRI) has become the leading imaging in the past ten years. This is mainly due to its ability to provide high level of resolution at a variety of different contrasts that reveal even the slightest difference between tissues accurately. Moreover, its ability to image functions as well as anatomy adds a new dimension to its use that is unique among other modalities. The acquisition speed of magnetic resonance imaging (MRI) is an important issue.

Increasing the acquisition speed shortens the total patient examination time; it reduces motion artifacts and increases the frame rate of dynamic MRI. Parallel MRI is a way to use multiple receiver coils with distinct spatial sensitivities to increase the MRI acquisition speed. The acquisition is speeded up by under sampling the k -space in the phase-encoding direction. The resulting data loss and consequent aliasing is compensated by the use of additional information obtained from several receiver coils.

In this thesis we explore a new methods for improving the current Parallel MRI techniques are studied. Comparison between conventional rapid MRI and PMRI is reviewed. A new method that improves the phase of the reconstructed images as well as produce a more uniform sensitivity images. Studying the factors that affect Parallel MRI performance and introduce analysis to describe the theoretical base for the widely current used algorithm the Generalized Auto calibrating Partially Parallel Acquisition (GRAPPA). And finally we introduce an innovative method that use the Parallel MRI combined with the Neural Network for Gridding the non-Cartesian samples within the k -space to overcome the current limitations associated with the currently used methods.

The proposed methodologies are implemented to reconstruct images from a Numerical phantom as well as real phantom data.

To my Family

ACKNOWLEDGEMENTS

All praises be to Allah who bestowed his blessings on my entire life and guided me for seeking knowledge. I am most grateful to my family “Dad, mom and my sisters” who have been supporting and encouraging during my entire life, giving me love, and care. I cannot help but dedicate this thesis to them.

I would like to appreciate the help and the support of Prof. Yasser Kadah. He has been a great advisor for me and supporting me on all steps till finishing this thesis the proper way. I have learned a lot from him not only on the scientific level but also on the personal and professional levels. I deeply appreciate his continuous support and encouragement during my life and studies.

My deepest thanks and appreciation to, my friend first and then my partner in all my work, Dr. Refaat Gabr who has been beside me and supporting me on all my life steps, professional and personal ones, he has a great impact on all my life. I have always enjoyed working with him. We always have discussions, sharing ideas and looking for challenges whatever it is, relying on GOD blessings, support, our team spirit and self confidence.

Many thanks go to my dear friend Dr. Tamer Basha, who has been supporting me and has always been a good listener to me when I needed to talk. My thanks go to Dr. Inas Yassin, whom I respect deeply regarding both scientific vision and discussion.

My special thanks go to Dr. Mohamed Waly, Eng. Ayman El-Hosseiny, Eng. Ashraf Abou el-leil, Mohamed El-Zeiny and Dr. Maged Fayeze for their sincere help and support.

I am thankful to all my friends and companions who have been supporting and encouraging during my studies especially the research group at the faculty.

Finally, this dissertation would not have been possible without the expert guidance Of my esteemed advisor, Prof. Yasser Kadah. He always listen to our ideas inspired us and build in us the spirit of the team work. Despite all the assistance provided by Prof. Kadah and others, I alone remain responsible for the content of the following, including any errors or omissions which may unintentionally remain.

LIST OF FIGURES

1.1 A proton rotates about its own axis.....	3
1.2 the magnetization vector is partially flipped towards the x-y plane.....	4
1.3 Slice Selection.....	6
1.4 Summary of a spin echo pulse sequence and Application.....	7
1.5 Data Space that is the analog version of k-space.....	8
1.6 K-Space, the Fourier Transform of Image.....	8
1.7 Turbo flash pulse.....	10
1.8 Partial K-space Acquisitions.....	11
1.9 The FSE pulse sequence.....	14
2.1 Body coil for conventional MRI scan.....	21
2.2 Basic concept of parallel MRI.....	22
2.3 Illustration of the basic SENSE.....	26
2.4 Single coil imaging.....	28
2.5 Imaging with an array.....	29
2.6 Illustration of the basic SMASH relation.....	32
2.7 Fully Fourier encoded k-space.....	34
2.8 Use of ACS lines in VD-AUTO-SMASH	35
2.9 Schematic description of an accelerated.....	37
2.10 in a sliding block reconstruction.....	38
2.11 Sliding blocks in GRAPPA.....	38
2.12 Schematic representation of the parallel reconstruction scheme.....	41
3.1 Schematic description of GRAPPA.....	44
3.2 GRAPPA reconstruction with the additional body coil.....	46
3.3 The modified reconstruction method with the body coil.....	46

3.4 A procedure for intensity correction.....	47
3.5 The sum-of-squares reconstruction of GRAPPA.....	48
3.6 The sum-of-squares reconstruction of GRAPPA.....	48
3.7 The sum-of-squares reconstruction of GRAPPA using only surface coils.....,	49
4.1 Schematic description of GRAPPA with an acceleration factor $R = 2$	54
4.2 The magnitudes of the Fourier transform of the ratio.....	56
4.3 Profiles through the center of the Fourier transform of the coil sensitivity.....	57
4.4 The reconstructed sum-of-squares images using GRAPPA	58
5.1 GROG gridding of non-Cartesian points.....	65
5.2 The architecture of supervised back propagated Neural Network.....	69
5.3 The proposed Neural Network algorithm.....	70
5.4 Show the reconstructed images.....	72
5.5 The difference between the reconstructed SOS.....	72
5.6 The difference between the reconstructed SOS image of GROG.....	73
5.7 The reconstructed images for the real phantom data.....	73
5.8 The difference between real phantom data using the nearest.....	74

CHAPTER 1

MR Introduction

1.1 Introduction

Magnetic resonance imaging (MRI) is considered to be the most important development in medical diagnosis since the discovery of x-ray 100 years ago. It has become one of the most powerful tools of radiology, now being applied to virtually every part of the body [1].

Nuclear magnetic resonance (NMR) is a chemical analytical technique that has been used for over 50 years. It is the basis for MRI. (The word nuclear had the false connotation of the use of nuclear material; thus, it was discarded from the MR lexicon and “NMR” was replaced by the phrase magnetic resonance imaging [MRI].)

One of the pioneers of NMR theory was Felix Bloch of Stanford University, who won the Nobel Prize in 1946 for his theories. He theorized that any spinning charged particle (like hydrogen nucleus) creates an electromagnetic field. The magnetic component of this field causes certain nuclei to act like a bar magnet. Experimental verification for the Bloch equations did not come until the early 1950s. By 1960, several companies began producing analytical instruments called NMR spectrometers. During the 1960s and 1970s; NMR spectroscopy became widely used in academic and industrial researches. In the late 1960s,

engineer-physician Raymond Damadian worked with NMR spectroscopy. He showed that malignant tissue has a different NMR spectrum from that of normal tissue.

The phenomenon of nuclear magnetic resonance was developed as an imaging technique in the early 1970's. Its non-ionizing characteristic makes it ideal for detailed study of anatomical structures. Present techniques in MRI can display:

- Chemical Differences between tissues as change in gray scale image (Tumor pathology).
- Coronaries & arteries and Vessels either in thin slices or 3D-images.
- Axial, Coronal, Saggital and Oblique images from a complete 3-Dimensional voxel data set (Head).
- Long slices, particularly in saggital view (spine).

1.1.1 Why MRI?

MRI has a number of features that makes it superior to any other imaging modality in certain applications. These features include:

- **Spatial and Contrast Resolution:** MRI has an optimum combination of both. Spatial resolution refers to the ability of a process to identify small, dense objects such as metal fragments and micro calcifications. Contrast resolution allows visualization of low-density objects with similar soft tissue characteristic.

- Multiplanar Imaging: MRI is able to obtain direct transverse, saggital, coronal, and oblique plane images.
- Magnetic Resonance Spectroscopy & Functional MR..

1.1.2 Overview of MRI physics

In MRI, low frequency radio waves (RF pulse) penetrate the tissue and reflect back off magnetized spins within the object. The patient first is placed in a magnetic field to establish a bulk magnetization; then a radio frequency pulse is applied to generate a detectable signal and the pulse is terminated allowing relaxation to occur and signal to be recorded [2].

Nuclear magnetic resonance can occur with many elements that have odd number of protons so there always existing one proton that is unpaired. These elements include ^1H , ^{14}N , ^{31}P , ^{13}C , and ^{23}Na . Hydrogen nucleus is used because it is the most abundant in the human body and it yields the strongest MR signal. That unpaired proton is pointing either north or south and gives a net magnetic field or a “magnetic dipole moment” MDM [1]. When that proton is placed in a large magnetic field B_0 , it begins to “wobble” or precess as shown in Fig. 1.1.

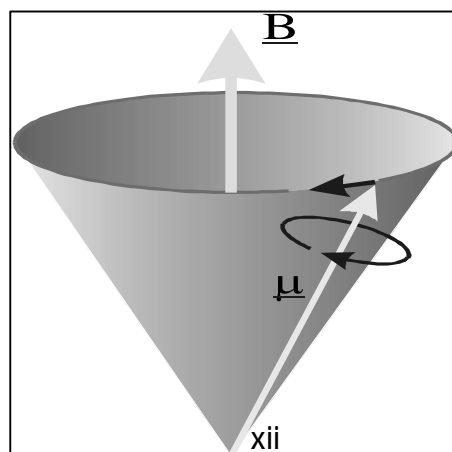


Figure 1-1. A proton rotates about its own axis and also about the axis of B₀.

The precession rate (ω_0) of the proton around the external magnetic field B_0 is given by Larmor Equation:

$$\omega_0 = \gamma * B_0$$

Where ω_0 = angular precessional frequency of proton, γ = gyro magnetic ratio, B_0 = strength of external magnetic field.

Initially all spins are lined up along the axis of the external magnetic field B_0 about which they are precessing. In a 3-dimensional (x, y, z) coordinate system, the direction of the external magnetic field always points to the z direction. Then an RF pulse (electromagnetic wave that results from brief application of an alternating electric current) is applied along the x-axis perpendicular to the magnetization vector M_0 , i.e. the axis of B_0 . The protons will begin to precess about the x-axis if the frequency of RF pulse matches ω_0 (i.e. satisfies Larmor Equation so resonance occurs). Which means that the vector M_0 (the net magnetization vector at the direction of the protons aligned along the external magnetic

field) begins to precess about the x-axis in the z-y plane as shown in Fig. 1.2. Depending on the strength of the RF pulse B_1 , and its duration τ , the flip angle is determined.

$$\theta = \gamma * B_1 * \tau$$

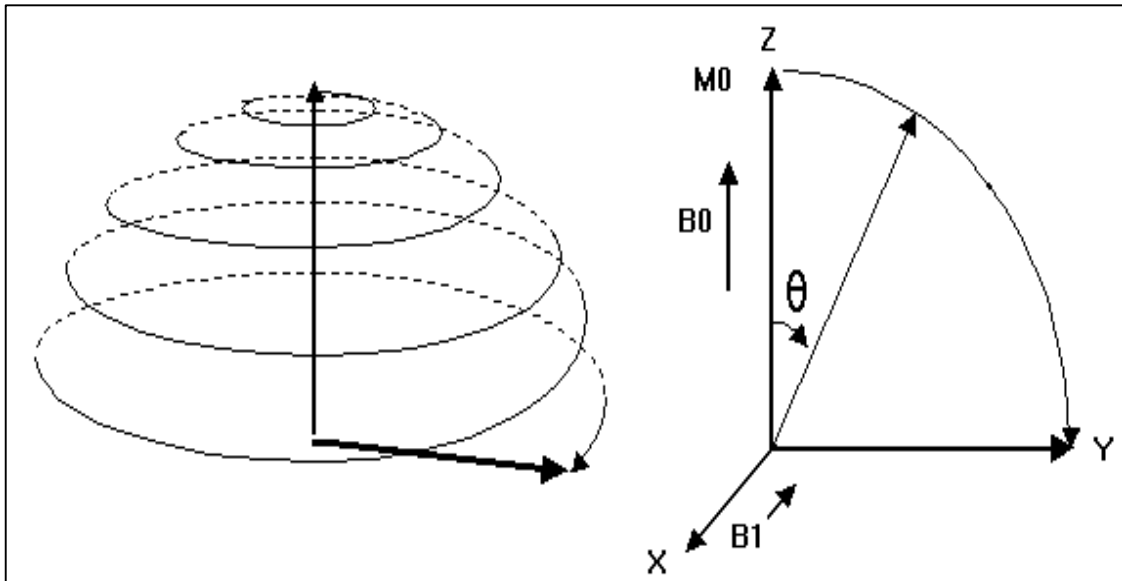


Figure.1-2. the magnetization vector is partially flipped towards the x-y plane

Relaxation is the process that occurs after terminating the RF pulse, in which the physical changes that were caused by the RF pulse return to the state they were in prior to the application of the pulse [1]. Re-growth of M_z along the z-axis is known as “T1 relaxation”, and decay of M_x in the x-y plane is known as “T2 relaxation”.

After applying 90° pulse (or any pulse sequence), another 90° pulse (or any pulse sequence) will be applied. The time between applications is called TR (The Repetition

Time). After applying RF, short period of time is to be waited before taking the measurement. This period of time is known as TE (Echo Time).

Three types of MR images can be produced depending on TR and TE:

- T1 weighted image, short TE and short TR are used.
- T2 weighted image, long TE and long TR are used.
- Spin density image, short TE and long TR are used.

1.1.3 Image Construction

The signals received from a patient contain information about the entire part of the patient being imaged. They do not have any particular spatial information. That is, the specific origin point of each component of the signal cannot be determined. This is the function of gradients. One gradient is required in each of the x, y, and z directions to obtain spatial information in that direction. Depending on their function, these gradients are called:

1. The slice-select gradient;
2. The read-out or frequency-encoding gradient; and
3. The phase-encoding gradient.

Depending on their orientation axis they are called G_x , G_y , and G_z . Depending on the slice orientation (axial, sagittal, or coronal).

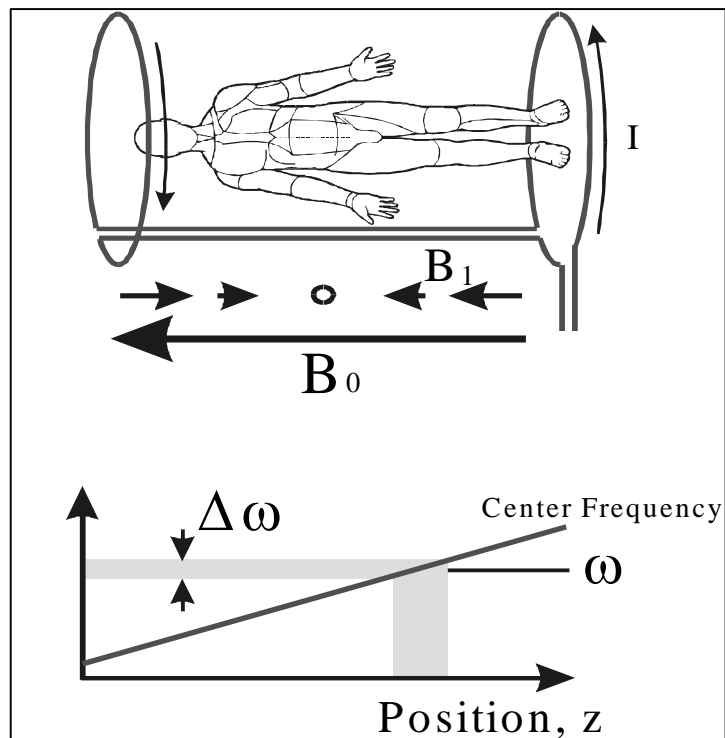


Figure 1-3. Slice Selection

A gradient is simply a magnetic field that changes from point-to-point usually in a linear fashion. The change in the magnetic field strength along the z-axis is called z gradient (G_z). For an axial slice in a super-conducting magnet, it is called slice select gradient as shown in

Fig. 1.3. After selecting a slice, to get spatial information in the x-direction of the slice another gradient is applied (G_x) during the time the echo is received i.e. during read-out. In addition another gradient is applied (G_y) in the y-direction. So the protons in each pixel will have a distinct frequency and a distinct phase, which are unique and encode for the x and y coordinates for that pixel.

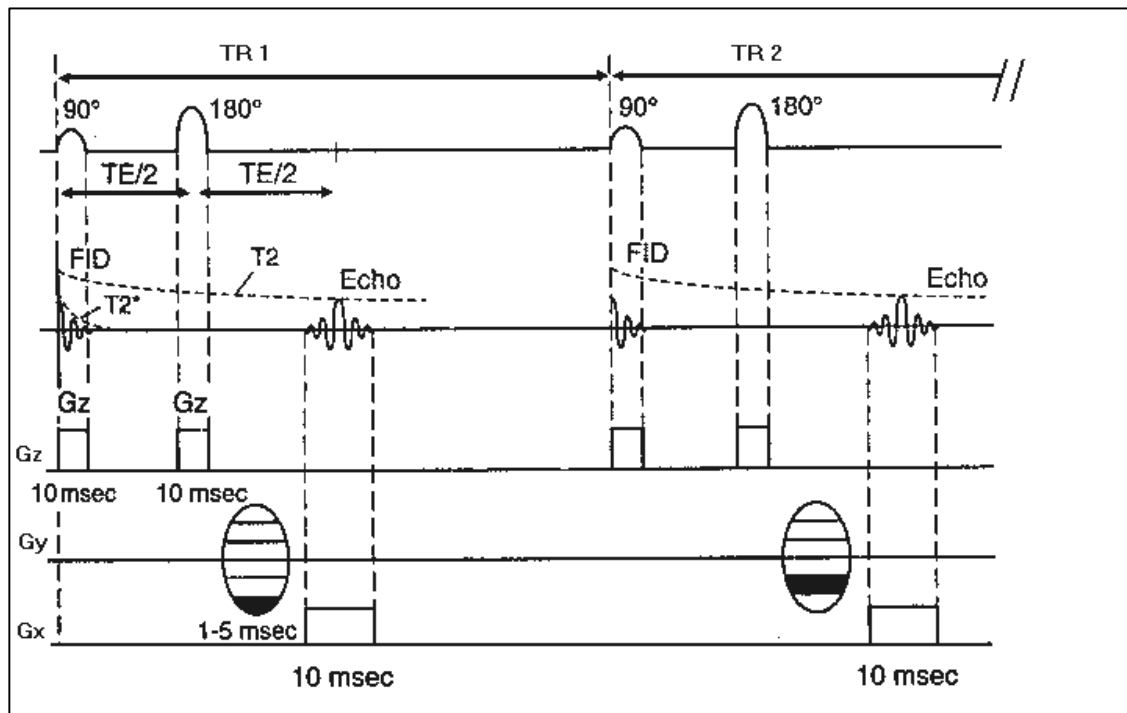


Figure.1-4. Summary of a spin echo pulse sequence and Application of G_x , G_y , and G_z .

These G_x , G_y , and G_z are applied in a specific way depending on the pulse sequence used. One of the most frequently used is the spin echo (SE) pulse sequence as shown in fig. 1.4. This sequence eliminates the effect of magnetic field inhomogeneity by an additional refocusing or rephasing 180° RF pulse [1].

Each received echo forms a line of the Data Space, “the analog version of k-space” as shown in fig. 1.5. After collecting the whole k-space, the MR image is formed by taking the Fourier transform of that k-space as shown in fig. 1.6.

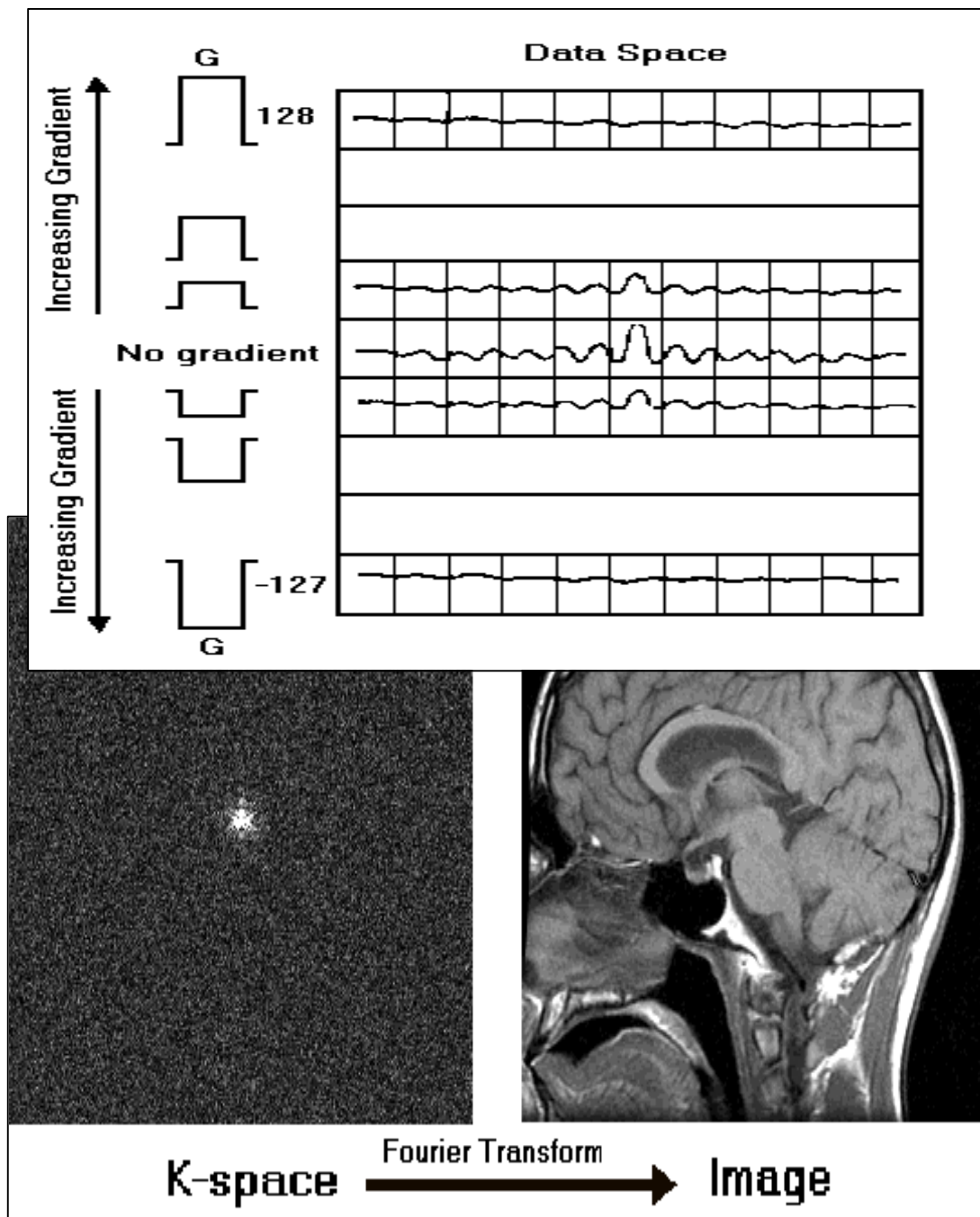


Figure 1-6. K-Space, the Fourier Transform of Image

1.1.4 Inversion Recovery sequences

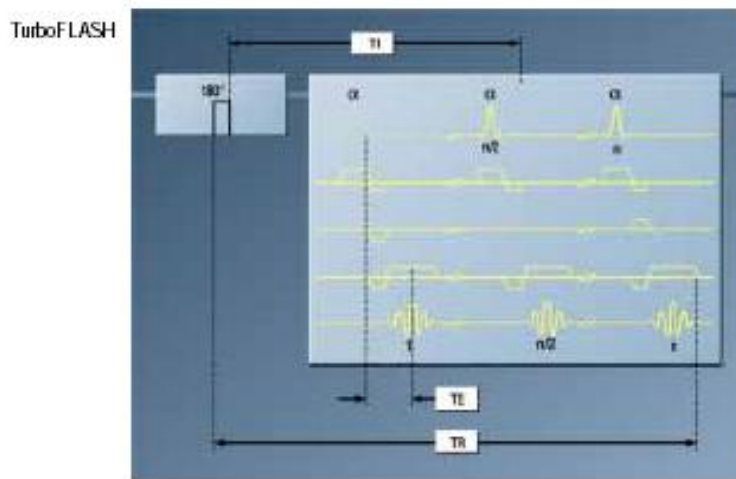
The spins are inverted by applying a 180° pulse. This means that they relax during inversion time TI. If the 90° excitation pulse is applied at the exact moment when the relaxation curve of a T1-value is at zero, the signal of this tissue is suppressed. This effect is of clinical relevance, in particular for fat suppression which requires a short TI (approximately 160 ms for 1.5 Tesla). The STIR method (Short TI Inversion Recovery) provides for effective fat suppression. Spin preparation not only eliminates the signal from fat, it also adds inverted T1 contrast to the image. Tissue with a long T1 appears brighter than tissue with a short T1.

1.1.5 Fast imaging with Turbo FLASH

Freezing physiological movement or performing dynamic perfusion series after injecting contrast agent, imaging in cine technique, and measurements of the abdomen and heart with a single breath hold: Turbo FLASH can do all that. Measurement times have been reduced to between a few hundredths of milliseconds and a few seconds. Even T1-weighted 3-D data sets with high resolution can be created within a short period of time. Motion artifacts are significantly reduced.

Turbo FLASH sequences comprise two phases; the preparation phase determines image contrast. Proton density contrast is produced through short repetition times and a small flip angle. A different type of image contrast is produced when other RF pulses are selected

prior to the acquisition phase. The entire raw data matrix is measured in a single step using an ultra fast gradient-echo sequence. The pulse interval in other gradient-echo sequences, the repetition time—is generally shorter than 10 ms. 128 lines are measured in approximately 1 second; therefore it is not useful to change this time. TR is therefore duration of a slice including the inversion pulse.



1.1.6 Figure.1-7 Turbo flash pulse sequence Partial Fourier Acquisitions

Partial Fourier imaging refers to MR acquisitions in which Fourier space is sampled asymmetrically around its origin. The missing data are either simply replaced by zeros, or they are calculated during the reconstruction process from the acquired data. The most commonly, data sampling in MR imaging uses a uniform sampling on to grid points Fourier. As the total imaging time is determined by the product of the number of phase-encoding steps and the repetition time, TR. The imaging time required to sample a 2D image (a) fully can be reduced by reducing the number of acquired phase encoding, (b). Alternatively, the minimum TR can be reduced by the acquisition of a partial echo (c) also

referred to as an asymmetric or fractional echo, which also reduces flow-induced artifacts. It is possible to combine both partial phase encoding and partial echo acquisition to further minimize imaging time

Some clinical applications require the preservation of the phase information throughout the reconstruction process, such as phase contrast imaging for velocity encoding, Dixon techniques for the separation of fat and water, and MR spectroscopy. If an MR image would consist of real components only, then it could be represented by half of its Fourier components and, thus, the acquisition time could be cut in half. In this case, the image would have no phase terms, and one half of the Fourier coefficients could be synthesized by the complex conjugate of the other half of Fourier space. This property is also called Hermitian symmetry. However, in practice, MR images do have phase terms induced by susceptibility effects at tissue boundaries, in homogeneities in the magnetic field, phase effects from flow and motion, eddy currents, data acquisition timing, and other sources as shown in Fig.1.8. Therefore, the acquisition of only half the k-space data with a reconstruction by conjugate symmetry or other means fails in practice. Instead, several algorithms have been developed to sample slightly more than half of k-space for a better phase estimate from these low spatial frequencies [3].

PARTIAL k -SPACE ACQUISITION

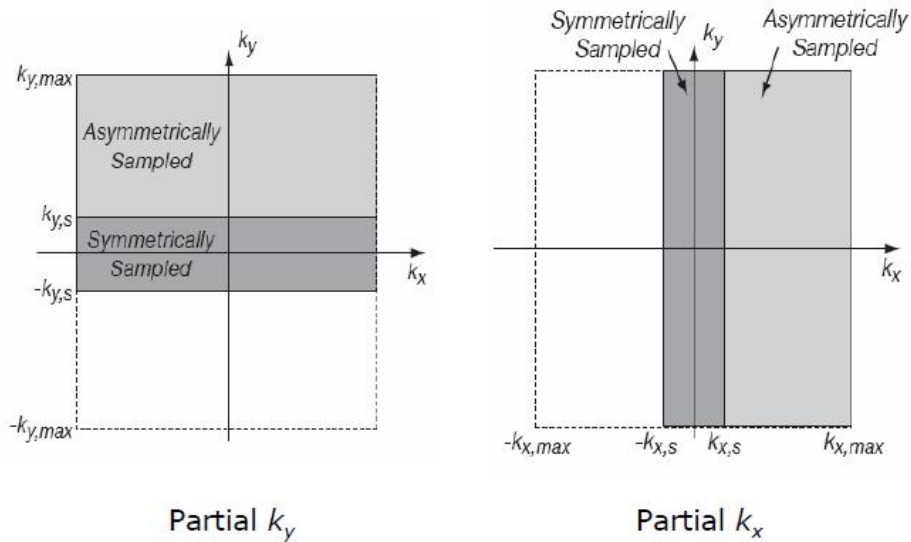


Figure 1.8 Partial K-Space Acquisitions

In the simplest approach, the missing k -space data are substituted by zeros prior to a standard image reconstruction. This zero-filling reduces the spatial resolution compared to a full acquisition and causes Gibbs ringing at sharp edges. However, the phase information of the image is preserved within the limits of the spatial resolution defined by the portion of k -space sampled on both sides of the origin. More advanced algorithms, synthesize the missing data and incorporate phase corrections based on the symmetrically sampled low-resolution data strip around the origin. They also introduce merging filters for smoother transitions from un-sampled to sampled data; thereby reducing ringing artifacts[3]. Within the limits of the accuracy of the phase estimate from the symmetrically sampled data portion, the Margosian and homodyne reconstructions[4] provide a spatial

resolution identical to the fully sampled data set. Compared to a full acquisition, the SNR is decreased because the total acquisition time has been reduced. This type of reconstruction leads to a loss of phase information and cannot be used for acquisitions that require a phase representation of the image data.

However, there are also residual errors in the homodyne reconstruction in the regions where the phase estimate from the symmetrically sampled data does not sufficiently describe the actual phase of the phantom. Alternatively, iterative methods [5] have been suggested, which potentially provide better phase estimates at regions with rapidly changing phase such as tissue boundaries with high susceptibilities. Additional imaging time savings can be accomplished with partial Fourier acquisitions in more than one dimension, e.g., in both phase-encoding directions in 3D imaging or with a combined fractional echo acquisition and partial Fourier sampling in the phase encoding direction. However, the missing data cannot be recreated with the 1D partial Fourier reconstruction methods discussed above, since only one quarter of k-space is properly sampled. Some imaging protocols offer double or even triple partial Fourier acquisitions combined with zero-filling of the missing data.

While the large time savings of such acquisitions are tempting and the image quality is usually pleasing, important diagnostic information can be obscured when not properly acquiring or synthesizing k-space data[5]. Recently proposed an iterative solution that can properly synthesize data for such acquisition strategies, though these iterative solutions are not used on clinical scanners.

1.1.7 Echo Planar Imaging (EPI)

EPI was used for real-time cardiac imaging in 1987 [1] bringing down the image scan time to 40msec with a resolution of 4mm. TR as seen earlier, is time between two acquisitions. This pulse sequence aims at reducing the time elapsed between two simultaneous acquisitions. The pulse sequence and the k-space coverage for EPI are shown in Figure 2-1. Improvements such as segmented or interleaved EPI [3] have been developed to improve the resolution to 2.6mm for 110msec of scan time. However, an EPI sequence is extremely difficult to implement practically. It is limited by the current hardware and the gradient switching speed. Some of the disadvantages of EPI are

1. Gradient systems: It is hard to get the correct gradient rise times for rapid switching.
2. Eddy currents: The gradient switching generates eddy currents in the MR hardware system and show up as artifacts in the image in the form of bright spots.
3. Field in homogeneity: Any spurious gradients generated due to the in homogeneities in the B₀ cause artifacts in the resultant image.
4. Chemical shift: This is the shift in the resonance frequency of the proton in two different chemical environments. For instance, the hydrogen protons in water and fat show a

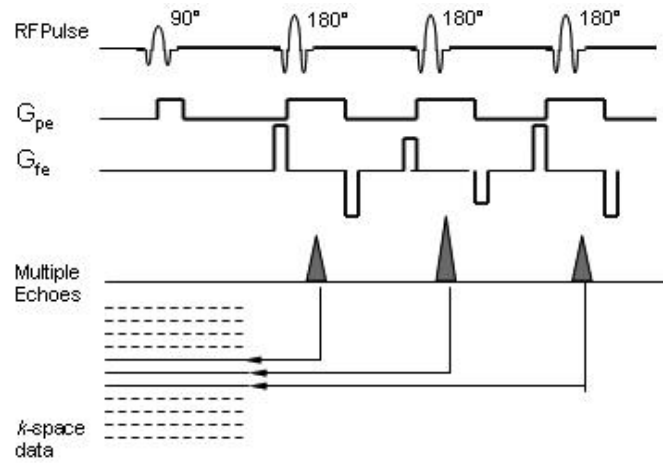
difference of around 3ppm due to the different molecules they are surrounded by at 1Tesla. This effect becomes more pronounced with higher gradients.

1.1.8 Fast Spin Echo (FSE)

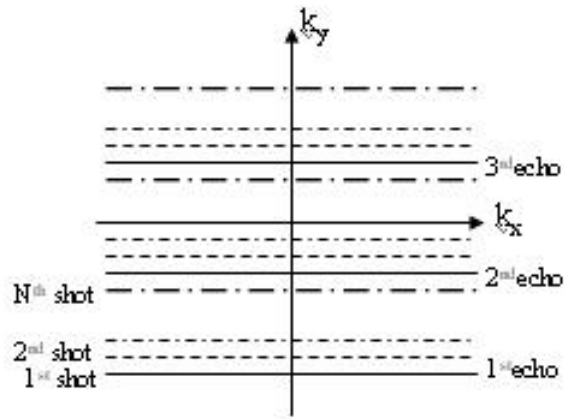
Fast Spin Echo is another pulse sequence used to facilitate rapid imaging. This sequence collects more lines per echo unlike the convention where only one line is collected for every RF excitation. Out of N k-space lines to be collected, if M lines are scanned per echo then the total acquisition time is reduced by N/M. The M lines collected per excitation are selected far away from one another so that their signals do not mix. The pulse sequence and the coverage are as shown in Fig.2-3. FSE has the following drawbacks:

1. Excess RF power: For acquiring multiple lines, multiple 180° pulses have to be applied causing a lot of RF power to be accumulated on the subject being imaged. The magnetization starts saturating and the signal strength decreases.
2. Different TE problem: Since the M lines are acquired at different times, each line in reality corresponds to a line from an image acquired at a different TE. The reconstructed image therefore corresponds to an approximate TE and may cause blurring.

3. T2 decay: As the phase encoding gradient applied for collection of each of the M lines is after considerable time gap, the T2 decay effect becomes prominent resulting in a blurring.



(a)



(b)

Figure 1-9: (a)The FSE pulse sequence, and (b) :the FSE k -space coverage (Figure modified from [4]).

1.2. MRI Artifacts

Artifacts refer to the appearance of something on the image, which does not represent or correlate with anything real in the volume of tissue being imaged. It is important to have the tools to eliminate or, at least, minimize them. These artifacts can be classified as follows [1, 2, 3]:

1.2.1. Magnetic and RF Field Distortion Artifacts

A. System Related

1. Primary static magnetic field:

The primary static magnetic field can never maintain perfect stability and may vary regionally from day to day.

2. Magnetic field gradient inhomogeneity.
3. RF coil inhomogeneity.
4. Gradient coil switching/timing accuracy.

Each of the components used to transmit and receive RF signals and manipulate the magnetic field gradients can do so with limited consistency. The images produced by surface coils and magnetic gradient imaging techniques (GE) are especially sensitive to magnetic field inhomogeneities.

B. Patient Related

1. Ferromagnetic materials:

Small metallic objects such as buttons, snaps, zippers, or batteries produce distortion. The typical ferromagnetic material artifact has a partial or complete loss of signal at the site of the metal. Such metal can distort the local magnetic field sufficiently so that the Larmor frequency for local spins is outside the frequency range of the imager. Furthermore, metal contains no hydrogen; the result is signal void at that location.

2. Body shape and conductivity:

The patient's shape, electrical conductivity, and filling of the radio frequency (RF) coil all become factors in creating inhomogeneity of the primary static field and the transmitted RF pulse.

3. Extension of body outside magnetic field:

Extension of a body part outside the area of maximum field homogeneity will frequently cause a metallic-like artifact at the edge of this area. This curvilinear artifact conforms to the shape of the magnetic field at the edges and may have a characteristic pattern for an individual magnet system.

4. Chemical shifts:

Chemical-shift artifacts are present wherever contiguous tissues have considerably different molecular organization. The artifact is seen as a bright rim of signal at one interface and a dark rim at the opposite side of the particular organ, oriented in the frequency-encoding direction. The most prominent examples seen are at interfaces of fat and the other body tissues.

1.2.2. Reconstruction Artifacts

A. System Related

1. Truncation:

The truncation or “ringing” artifact appears as multiple, well-defined curved lines regularly conforming to the anatomic boundary. The truncation artifact is more pronounced when the number of phase-encoding acquisitions is small and the reconstruction matrix is asymmetric. It occurs in areas where there is a great difference in signal intensity, such as interfaces of fat and air or fat and cortical bone.

2. Quadrature detection:

A zero line or zipper artifact is caused by RF feed through from the RF transmitter along the frequency-encoding direction at the central or reference frequency of the imaging sequence. The result is a segmented line extending across the middle of the field of view in the frequency-encoding direction and having a zipper-like appearance.

B. Patient Related

1. Aliasing (wraparound):

The Aliasing artifact is one of the most commonly encountered of this group. It occurs when portion of the patient’s body are outside the field of view but within the area of RF excitation. When hydrogen nuclei outside the area of interest are excited, the signal they return is interpreted to have originated from within the imaging field of view. It is then projected over the real portion of the image on the opposite side of its actual location.

2. Partial volume averaging:

Partial volume averaging results whenever the particular structure of interest is contained within two contiguous slices. The use of thin slices reduces this artifact. However, thin slices acquisition need more time. Furthermore the adequacy of the manufacturer's magnetic gradient coils may not be equal to the task of precisely defining such thin slices.

1.3 Thesis Objective

Magnetic Resonance Imaging (MRI) is a relatively new technique for medical imaging. MRI is a non-invasive technique, it offers various contrast methods and it produces no radiation. The disadvantage is the high utilization and acquisition cost. The device also needs to be situated in a radio-waves prove room. However, the most important weakness of MRI is acquisition time. The prolonged acquisition process is unpleasant for patients, it is source of motion artifacts and it simply limits the amount of data that can be measured. Applications such as real-time cardiac imaging, functional brain imaging, contrast enhanced MRI require fast scan. The reason why acquisition time is so long is that MRI is performed in a strictly sequential fashion using magnetic gradients to spatially encode the signal position. The bottleneck of the acquisition time is the time that takes to acquire one line in k-space in phase-encoding direction. There are several techniques currently in use that increase the speed of the acquisition in phase encoding direction. It is done by improving the magnitude and the switching rate of the magnetic gradient fields. However, there are physical limits that could not be exceeded.

Besides the image contrast, imaging speed is probably the most important consideration in clinical magnetic resonance imaging (MRI). Unfortunately, current MRI scanners already operate at the limits of potential imaging speed because of the technical and physiologic problems associated with rapidly switched magnetic field gradients. With the appearance of Parallel MRI (PMRI), a decrease in acquisition time can be achieved without the need of further increased gradient performance. PMRI works by taking advantage of spatial

sensitivity information inherent in an array of multiple receiver surface coils to partially replace time-consuming spatial encoding, which is normally performed by switching magnetic field gradients. In this way, only a fraction of phase-encoding steps have to be acquired, directly resulting in an accelerated image acquisition while maintaining full spatial resolution and image contrast. Besides increased temporal resolution at a given spatial resolution, the time savings due to PMRI can also be used to improve the spatial resolution in a given imaging time. Furthermore, PMRI can diminish susceptibility-caused artifacts by reducing the echo train length of single- and multi-shot pulse sequences. Over the last 10 years, great progress in the development of PMRI methods has taken place, thereby producing a multitude of different and somewhat related parallel imaging reconstruction techniques and strategies. Currently, the most well known are SMASH, SENSE, and GRAPPA. However, various other techniques, such as AUTO-SMASH, VD AUTO-SMASH, Regularized SENSE, PILS, and SPACE RIP have also been proposed. All these techniques require additional coil sensitivity information to eliminate the effect of under sampling the k-space. This sensitivity information can be derived either once during the patient setup by means of a pre-scan or by means of a few additionally acquired k-space lines for every subsequent PMRI experiment (auto-calibration), or some combination of the two.

In this thesis, we will explore new methods for the acquisition and reconstruction of MRI data in order to improve the final reconstructed image. The first problem we will address is the shading artifact which results when combining images from different coils with different coil sensitivities. This will be related to the conventional sum of squares

reconstruction, wherein the phase information is also lost. We will develop a method that will produce complex images and at the same time will show more uniform sensitivity (less shading) over the entire field of view.

We also introduced an explanation that can describe the theoretical and basic principles for the most used parallel imaging algorithm into the k-space, GRAPPA. That will lead to a new coil-specific variable kernel that can be used for reconstruction based on coil to coil interaction within the field of view.

Finally we show the potential of the parallel imaging in other applications like gridding, where we describe a new technique that combines parallel imaging with the neural network technique to grid non-Cartesian data acquired by an array of coils. We will compare the results to current techniques.

All methods developed in this dissertation will be developed theoretically and tested on both numerical and real data phantoms.

CHAPTER 2

Parallel Magnetic Resonance Imaging

In this chapter we will review the basic principles of the Parallel magnetic resonance imaging techniques, demonstrating the mathematical principles, different techniques,

The requirements, advantage and the disadvantage

2.1. Basic Concept

Unlike a conventional MRI scanner, parallel MRI requires an array of receivers to collect data simultaneously. Thus each coil is only locally sensitive as shown in Fig.2.1. In other words, with a receiver placed near a subject, the signal contributed by the subject to the receiver varies according to the relative position of the subject from the receiver. Thus, though every receiver collects the same k -space data, each one contains different information about the image.

In parallel MRI, data collected by each receiver element in k -space is subsampled data. Therefore, individual aliased images are obtained for every coil. These images are either unfolded in the image domain to yield the final image or the missed k -space lines are reconstructed using a priori information in the form of the spatially varying coil sensitivity distribution.

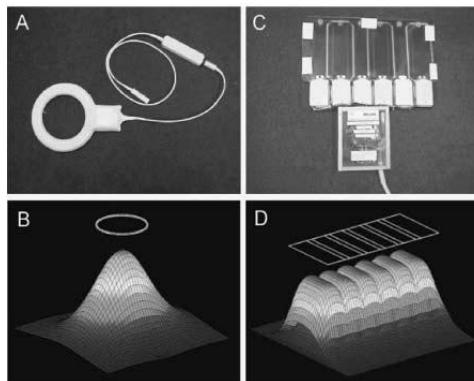


Figure 2.1 A: Body coil for conventional MRI scan, B: Coverage of body coil, C: Array of receivers for parallel MRI, D: Coverage of the array, each acquired a fraction of the total image. [6]

Consider for instance, two coils instead of the regular volume coil with sensitivities as shown in Fig 2-2. Then each coil acquires only half of the image since it receives strong signal from areas it is closest to and low or no signal from points away from it.

This effectively reduces the coil field of view (FOV) to half that of the image. If the individual coil data now were subsampled in k -space by a factor of 2, two halves of the image can be obtained simultaneously from the two coils. Once the two images are appropriately reconstructed after data acquisition, they can be combined to get the entire image. Various algorithms have been developed for correct image reconstruction and can be classified [7] as

- *Image domain based reconstruction:* Reconstruction is done by unfolding every image using the coil maps. For e.g., SENSitivity Encoding (SENSE) [9], partially Parallel Imaging with Localized Sensitivities (PILS) [9].
- *K-space based method: Reconstruction* is done by regenerating the missed k-space lines either for the ideal image or for individual coil images. For e.g. SiMultaneous Acquisition of Spatial Harmonics (SMASH)[10] AUTOcalibrating SMASH (AUTO-SMASH) [11], Variable density AUTO-SMASH (VD-AUTOSMASH) [12], GeneRalized Autocalibrating Partially Parallel Acquisitions (GRAPPA) [13].

- *Hybrid reconstruction:* Reconstruction is done partly in the image domain and partly in k -space. For e.g., Sensitivity Profiles from an Array of Coils for Encoding and Reconstruction In Parallel (SPACE RIP) [14].

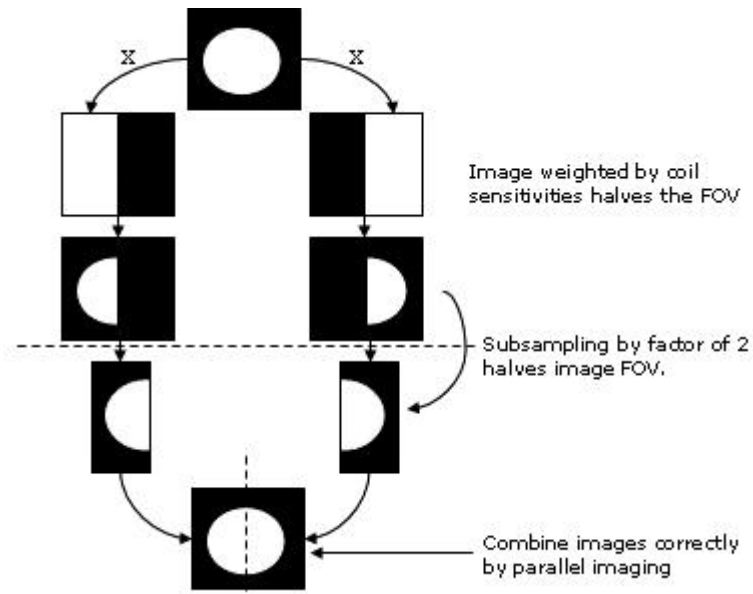


Figure 2-2 Basic concept of parallel MRI [7].

2.2. Sensitivity Encoding (SENSE)

To date, the most widespread used parallel MRI technique is SENSE, which is offered by many companies in slightly modified implementations: Philips (SENSE), Siemens (mSENSE) and GRAPPA, General Electric (ASSET), and Toshiba (SPEEDER). Because of the broad availability of SENSE, this technique has become the most used parallel imaging method in the clinical routine. Many clinical applications already benefit from the enhanced image acquisition capabilities of SENSE.

For example, in cardiac imaging, the scan time reduction due to SENSE relaxes the requirements for breath-hold studies. Optionally, the gain in scan time can be used to improve the spatial resolution. Furthermore, because of the reduced imaging time, real-time cardiac imaging without ECG triggering or breath-holding can be realized. Another example for the application of SENSE is contrast enhanced magnetic resonance angiography (CE-MRA). The most critical parameter for CE-MRA is the imaging time because the total acquisition has to be completed during the first pass of the contrast agent and therefore the spatial resolution of CE-MRA is restricted. SENSE enables a higher spatial resolution at constant scan time or a time-resolved CE-MRA study, consisting of multiple 3D data sets acquired during the passage of the contrast agent. A particular example of a clinical application that can benefit from the increased imaging speed provided by parallel imaging is head MRI.

Single-shot and turbo spin-echo sequences, such as TSE and HASTE, are commonly used for T_2 -weighted brain imaging. The application of parallel MRI can be used to effectively reduce blurring due to the T_2 relaxation and therefore improves the image quality of these sequences. Besides T_2 -weighted imaging with TSE sequences, single-shot echo-planar imaging (EPI) has become the clinical standard in areas such as functional MRI, diffusion-tensor imaging for fiber tracking, and diffusion-weighted MRI, which is an important diagnostic tool for the examination of patients with acute stroke. Combining single-shot EPI with SENSE has been shown to reduce the disadvantages of EPI, namely, the blurring and signal losses due to the T_2^* -based signal decay during read-out and distortions in the reconstructed image caused by off-resonance spins .

For breast imaging, magnetic resonance in combination with parallel imaging is a powerful diagnostic tool, which also yields functional information about a breast cancer's biologic behavior and might become a standard, frequently used, clinical study in the near future. In particular, dynamic contrast enhanced breast MRI benefits from a higher spatial resolution at a given scan time provided by SENSE. The increased spatial resolution allows the visualization of high anatomic detail and therefore delivers an increased diagnostic specificity [7].

2.2.1. Sensitivity Encoding With Cartesian Sampling of k-Space.

In two-dimensional (2D) Fourier imaging with common Cartesian sampling of k -space, sensitivity encoding by means of a receiver array permits reduction of the number of Fourier encoding steps. This is achieved by increasing the distance of sampling positions in k -space while maintaining the maximum k -values. Thus scan time is reduced at preserved spatial resolution. The factor by which the number of k -space samples is reduced is referred to as the *reduction factor* R . In standard Fourier imaging, reducing the sampling density results in the reduction of the FOV, causing aliasing. In fact, SENSE reconstruction in the Cartesian case is efficiently performed by first creating one such aliased image for each array element using discrete Fourier transform (DFT).

The second step then is to create a full-FOV image from the set of intermediate images. To achieve this one must undo the signal superposition underlying the fold-over effect. That is, for each pixel in the reduced FOV the signal contributions from a number of positions in the full FOV need to be separated.

A pMRI accelerated acquisition (reduction factor R) results in a reduced FOV in every component coil image. Each pixel in the individual reduced FOV coil image will contain information from multiple (R), equidistantly distributed pixels in the desired full FOV image. Additionally, these pixels will be weighted with the coil sensitivity C at the corresponding location in the full FOV. Thus, the signal in one pixel at a certain location (x, y) received in the k *th* component coil image I_k can be written as

$$I_k(x, y) = C_k(x, y_1)p(x, y_1) + \dots + C_k(x, y_R)p(x, y_R). \quad (2.1)$$

With index k counting from 1 to N_c and index l counting from 1 to R , specifying the locations of the pixels involved, Equation 1 can be rewritten to

$$I_k = \sum_{l=1}^{Np} C_{kl} P_l. \quad (2.2)$$

Including all N_c coils, a set of (N_c) linear equations with (R) unknowns can be established and transformed in matrix notation:

$$\vec{I} = \hat{C} \cdot \vec{p}. \quad (2.3)$$

As shown in Fig.2.3, the vector \vec{I} represents the complex coil image values at the chosen pixel and has length N_c . The matrix \hat{C} denotes the sensitivities for each coil at the R *superimposed* positions and therefore has the dimension $N_c \times R$. The vector \vec{p} lists, the R pixels in the full FOV image. Using proper knowledge of the complex sensitivities at the

corresponding positions, this can be accomplished using a generalized inverse of the sensitivity matrix \hat{C} .

$$\bar{p} = (\hat{C}^H \hat{C})^{-1} \hat{C}^H \cdot \bar{I}. \quad (2.4)$$

To simplify matters, the issue of noise correlation is not addressed in Eq.2.4. However, to account for levels and correlations of stochastic noise in the received data, terms may be included to deal with this correlation. This can be especially important when the receiver coils are not completely decoupled. A detailed description is given by [8].

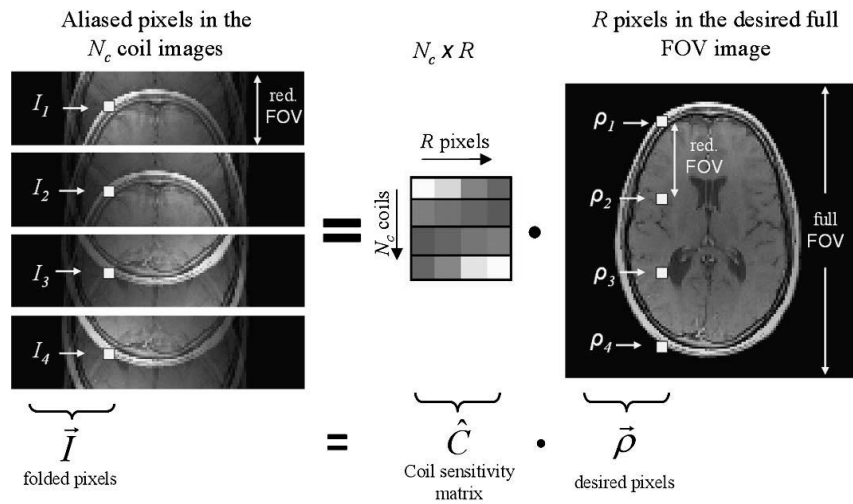


Figure 2.3 Illustration of the basic SENSE relation using an accelerated ($R=4$) pMRI acquisition with

$N_c = 4$ receiver coils. \bar{I} Contains the aliased pixels at certain positioning the reduced FOV coil

images. The sensitivity matrix \hat{C} assembles the corresponding sensitivity values of the component coils at the locations of the involved ($R=4$) pixels in the full FOV image \bar{p} .

The “unfolding” process in Eq. 2.4 is possible as long as the matrix inversion in Eq.2.4 can be performed. Therefore, the number of pixels to be separated R must not exceed the number of coils N_c in the receiver array. The SENSE algorithm (Equation 3.4) has to be repeated for every pixel location in the reduced FOV image to finally reconstruct the full FOV image. SENSE provides pMRI with arbitrary coil configurations, however, at the expense of some additional SNR loss, which depends on the underlying geometry of the coil array. The encoding efficiency at any position in the FOV with a given coil configuration can be analytically described by the so-called geometry factor (g factor), which is a measure of how easily the matrix inversion in Eq.2.4 can be performed. Thus, the SNR in the final SENSE image is additionally reduced by the g -factor.

$$SNR_{SENSE} = \frac{SNR_{full}}{\sqrt{R \cdot g}}. \quad (2.5)$$

2.3. Regularized SENSE

Reconstruction using SENSE gives a poor image due to inaccurate estimation of the coil geometry causing the reconstruction matrix to be ill-conditioned [15]. SNR is further reduced in SENSE due to this condition. Tikhnov regularization [16] is done to make use of the low resolution coil maps as a priori information. Error due to noise and ill

conditioning is appropriately weighted using the regularization parameter λ . Selection of correct λ is important for noise suppression in Regularized SENSE.

$$I_{reg} = I_{rec} + (((S^H \times S + \lambda^H \times \lambda)^{-1}) \times S) \times (I_{prior} - S \times I_{rec}), \quad (2.6)$$

Where I_{reg} is the regularized image, I_{rec} is the reconstructed image, S is the coil sensitivity matrix and λ is the regularization parameter.

2.4. Partially Parallel Imaging with Localized Sensitivities (PILS)

2.4.1. Review of some basics of the phase encoding process.

Before discussing the details of the PILS technique, we first review some basics of the phase encoding process used in traditional imaging methods. In conventional Fourier transform (FT) imaging, k -space is sampled at a spacing of Δk_y so that the Nyquist Criterion is satisfied for the width of the object, Y Fig. 2.4a. We can define an imaging FOV Y_i which corresponds to the FOV sampled along the phase encoding direction. If, for example, the FOV Y_i is chosen to be a factor of two smaller than Y , image aliasing is typically observed along the phase encoding direction Fig. 2.4b.

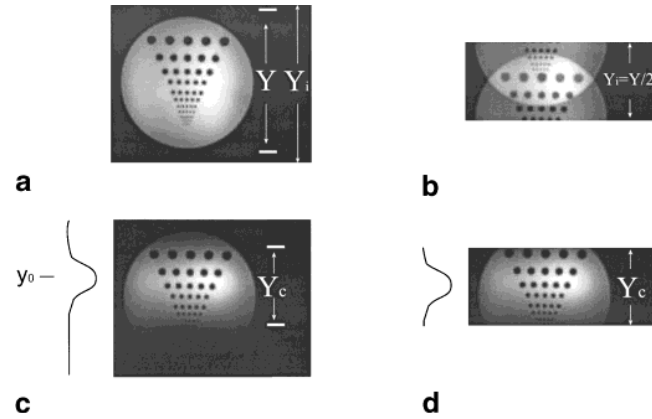


Figure 2.4 Single coil imaging. a: Definition of the object width Y and the imaging FOV Y_1 . b: If a FOV of $Y/2$ is used in the acquisition, image aliasing results. Information is lost in this case due to the overlapping of spatial information. c: Imaging with a surface coil restricts the bandwidth of the signal to a range Y_c centered around y_0 . d: When a surface coil is used for imaging, the FOV in the phase encoding direction can be reduced to Y_c instead of Y without aliasing problems.

The statements given above assume that an RF coil with uniform sensitivity is used for reception. Image aliasing can be prevented if a coil with local sensitivity is used, such as a surface coil. In this situation, we can treat the RF coil as an analog filter along phase encoding direction that limits the signal to the local imaging FOV Y_c along the phase encoding direction Fig.2.4c. Therefore in the case of this single surface coil, Δk_y can be chosen to sample the FOV Y_c instead of Y Fig.2.4d. Since this image has a smaller FOV,

it requires fewer samples compared to the full FOV and can therefore be acquired in a reduced time.

Here we define the *acceleration factor* as the ratio of the sampling spacing in k -space needed to sample the full FOV image divided by the sampling spacing used in the small FOV acquisition. This parameter gives the ratio of speed improvement that is obtained using the smaller FOV acquisition instead of the larger FOV acquisition.

The basic idea in PILS is to take this concept of reduced FOV acquisitions in a single coil, and apply it to acquisitions in which smaller FOV images are acquired in parallel in each element of the array. In PILS we view an array of surface coils as a bank of filters, each with a FOV of Y_c , but with a different offset y_0 which span Y Fig.2-5a. The primary idea of PILS is to simultaneously collect images in each coil with an FOV of Y_i (less than Y), each corresponding to a different sub region of the full FOV image. We then use the PILS reconstruction process to combine these local image acquisitions into an image with a composite width Y .

To see how the PILS reconstruction process works, we begin with the assumption that each coil has a completely localized sensitivity, such that each coil has sensitivity over Y_c , and is zero everywhere else. The process begins with the acquisition of an image with FOV Y_i simultaneously in each coil of the array, where Y_c, Y_i, Y . As can be seen from Fig 2.5b, as long as Y_i is chosen to be larger than Y_c , the periodically repeating sub-images are

completely separated, although the position of the correct sub-image is lost. The primary goal of the PILS reconstruction process is to reconstruct only the sub-image which is in the correct position in each coil of the array [9]. This process is described in the next section.

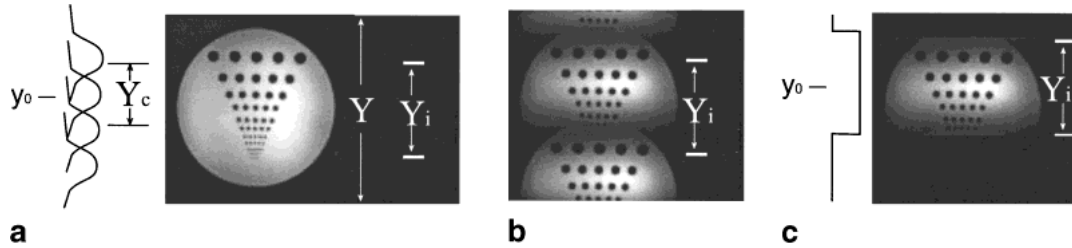


Figure 2-5 Imaging with an array. **a:** Definition of Y_c , y_0 and Y_i for an array which spans a length Y .

b: If an image is acquired with a FOV of Y_i , which is bigger than Y_c , but less than Y , several repeating subimages appear in the full FOV reconstruction, however no overlapping of spatial information occurs, due to the inherent filtering of the surface coil. **c:** In PILS, information about the center position of the signal is incorporated into the reconstruction, and all signal from outside the correct region is suppressed. This results in the correct full FOV image in each component coil.

2.4.2. PILS Reconstruction Algorithm

We begin with the simple 1D Fourier transform representation of the MR signal:

$$S(k_y) = \int_{-\infty}^{\infty} p(y) \cdot e^{ik_y y} dy, \quad (2.7)$$

Where $p(y)$ is the spin density of the sample along the phase encoding direction and $S(k_y)$ is the received signal. However, if we assume that a coil with localized sensitivity limits the signal to an FOV of Y_c centered around y_0 , this integration reduces to:

$$S(k_y) = \int_{y_0 - Y_c/2}^{y_0 + Y_c/2} p(y) \cdot e^{ik_y y} dy. \quad (2.8)$$

In the PILS reconstruction, it is assumed that we already have knowledge of the correct location of the center of the coil's sensitive region y_0 and the acceleration factor used in the data acquisition. Using this prior knowledge of the range of y values that actually contributed signal in Eq.2.8, we can restrict the reconstruction to only have signal

in the predefined range of y where the signal originated, such that over the range $y_0 - Y_i / 2 < y' < y_0 + Y_i / 2$,

$$p(y') = \sum_{k_y} S(k_y) \cdot e^{-ik_y y'} = FFT\{\varphi(k_y)S(k_y)\}. \quad (2.9)$$

And is zero everywhere else Fig.2.5c. The term $\varphi(k_y)$ is a simple linear phase term needed to correctly shift the center of the reconstructed data to the center of the reconstruction window and is given by:

$$\varphi(k_y) = e^{ik_y y_0}. \quad (2.10)$$

Repeating this process for each coil results in unaliased full FOV images for each coil with signal only in the predefined regions. A composite image can then be reconstructed using any conventional method, such as a sum of squares reconstruction. Many issues need to be considered before this technique can be implemented in practice. Foremost among these issues is the validity of our assumption that the surface coils in the array provide localized sensitivities and that their spatial location can be determined accurately [9].

2.5. SMASH

Like SENSE, pure SMASH (Simultaneous Acquisition of Spatial Harmonics) at its basic level requires a prior estimation of the individual coil sensitivities of the receiver array. The basic concept of SMASH is that a linear combination of these estimated coil sensitivities can directly generate missing phase-encoding steps, which would normally be performed by using phase-encoding magnetic field gradients. In this case, the sensitivity values $C_k(x, y)$ are combined with appropriate linear weights $n_k^{(m)}$ to generate composite sensitivity profiles C_m^{comp} with sinusoidal spatial sensitivity variations of the order m Fig 2.6 :

$$C_m^{comp}(x, y) = \sum_{k=1}^{N_c} n_k^{(m)} c_k(x, y) \cong e^{im\Delta k_y y}. \quad (2.11)$$

Here, $\Delta k_y = 2\pi / FOV$ and index k counts from 1 to N_c for an N_c -element array coil, while m is an integer, specifying the order of the generated spatial harmonic. With this, the only unknowns in the linear equation are the linear weights $n_k^{(m)}$, which can be estimated by fitting (e.g. least square fit) the coil sensitivity profiles C_k to the spatial harmonic $e^{im\Delta k_y y}$ of order m . The component coil signal $S_k(k_y)$ in one dimension (phase encoding direction), which is received in coil k , is the Fourier transformation of the spin density $\rho(y)$ weighted with the corresponding coil sensitivity profile $C_k(y)$:

$$S_k(k_y) = \int dy \rho(y) C_k(y) e^{ik_y y}. \quad (2.12)$$

Using Eq.2.11 and 2.12, we may derive an expression to generate shifted k-space lines $S(k_y + m\Delta k_y)$ from weighted combinations of measured component coil signals $S_k(k_y)$.

$$\sum_{k=1}^{N_c} n_k^{(m)} \cdot S_k(k_y) = \int dy \rho(y) \sum_{k=1}^{N_c} n_k^{(m)} C_k(y) e^{ik_y y} \quad (2.13)$$

$$\cong \int dy \rho(y) e^{im\Delta k_y y} e^{ik_y y} = S^{comp}(k_y + m\Delta k_y).$$

Eq. 2.13 represents the basic SMASH relation and indicates that linear combinations of component coils can actually be used to generate k-space shifts in almost the same manner as magnetic field gradients in conventional phase-encoding. In general, though, SMASH is strongly restricted to coil configurations that are able to generate the desired spatial harmonics in phase-encoding direction with adequate accuracy Fig.2.6 [7, 10].

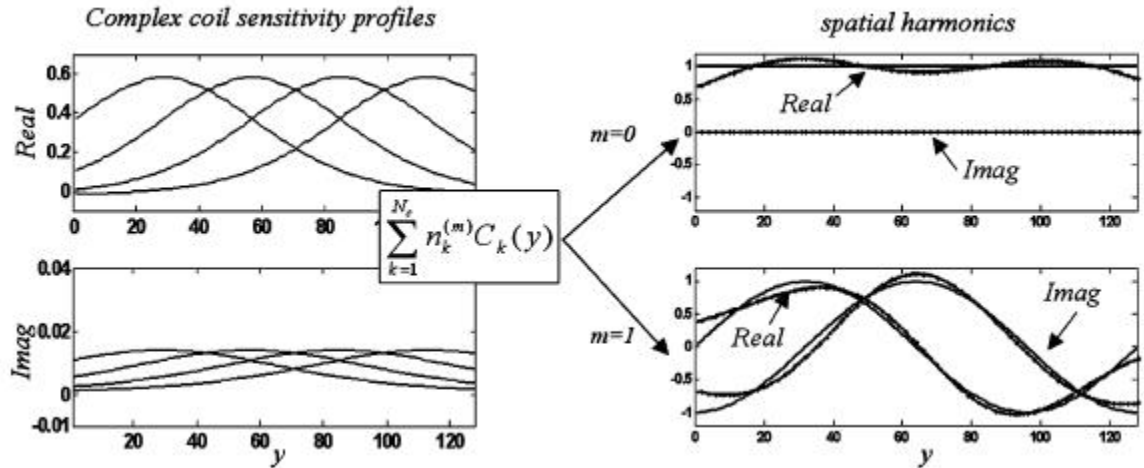


Figure 2-6 Illustration of the basic SMASH relation. The complex sensitivity profiles $C_k(y)$ from a 4-element ideal array (left) are fit to spatial harmonics (solid lines) of order $m = 0$ (right top) and $m = 1$ (right bottom). The dotted lines represent the best possible approximation of the spatial harmonics with the underlying coil array.

2.6. Auto-SMASH and VD-AUTO-SMASH

In contrast to a prior estimation of component coil sensitivities, AUTO-SMASH uses a small number of additionally acquired AutoCalibration Signal (ACS) lines during the actual scan to estimate the sensitivities. An AUTO-SMASH type acquisition scheme is shown in Fig.3.7c for a reduction factor $R = 3$. In general, $R - 1$ extra ACS lines are required, which are normally placed in the center of k-space at positions $m\Delta k_y$, where m counts from 1 to $R - 1$. In contrast to normal SMASH, these additionally acquired ACS lines S_k^{ACS} are used to automatically derive the set of linear weights $n_k^{(m)}$.

In the absence of noise, the combination of the weighted profiles at (k_y) of the component coil images that represents a k-space shift of $m\Delta k_y$ must yield the weighted (by the 0th harmonic factor) combined autocalibration profile obtained at $k_y + m\Delta k_y$,

$$S^{comp}(k_y + m\Delta k_y) = \sum_{k=1}^{N_c} S_k^{ACS}(k_y + m\Delta k_y) \cong \sum_{k=1}^{N_c} n_k^{(m)} S_k(k_y). \quad (2.14)$$

By fitting the component coil signals $S_k(y)$ to the composite signal $S^{comp}(k_y + m\Delta k_y)$, which are composed of ACSs $S_k^{ACS}(k_y + m\Delta k_y)$, a set of linear weights $n_k^{(m)}$ may again be derived, which can shift measured lines by $m\Delta k_y$ in k-space. In this way, missing k-space data can be calculated from measured k-space data to form a complete dense k-space, resulting in a full FOV image after Fourier transformation.

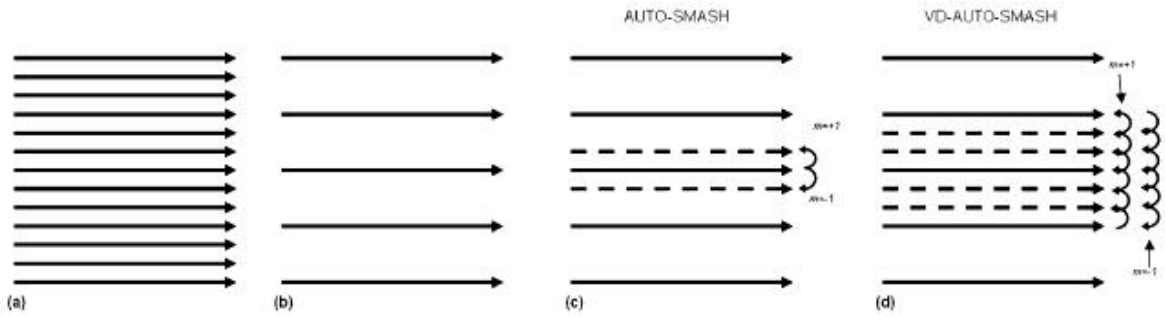


Figure 2-7 (a) Fully Fourier encoded k-space ($R = 1$), (b) undersampled ($R = 3$) k-space without ACS lines, (c) AUTO-SMASH-type undersampled ($R = 3$) k-space with two additional ACS lines to derive the coil weights for a k-space shift of $+\Delta k(m = +1)$ and $-\Delta k(m = -1)$, and (d) VD-AUTO-SMASH-type undersampled ($R = 3$) k-space with multiple additional ACS lines to derive the coil weights for a k-space shift of $+\Delta k(m = +1)$ and $-\Delta k(m = -1)$ more accurately.

The concept of variable-density (VD)-AUTO-SMASH was introduced as a way to further improve the reconstruction procedure of the AUTO-SMASH approach. In this method, multiple ACS lines are acquired in the center of k-space. Figure 3-7d schematically depicts a VD-AUTO-SMASH type acquisition with a threefold undersampled (outer) k-space. This simple examples demonstrates that the number of available fits with which one can

derive the weights for the desired k-space shifts ($m = +1, -1$) is significantly increased just by adding a few extra ACS lines to the acquisition. Furthermore, these reference data can be integrated in a final reconstruction step to further improve image quality. It has been shown [12] that the VDAUTO-SMASH approach provides the best suppression of residual artifact power at a given total acceleration factor R , using the maximum possible undersampling in the outer k-space in combination with the highest possible number of ACS lines in the center of k-space.

This strategy results in a more accurate determination of the reconstruction coefficients, especially in the presence of noise and a more robust image reconstruction in the presence of imperfect coil performance.

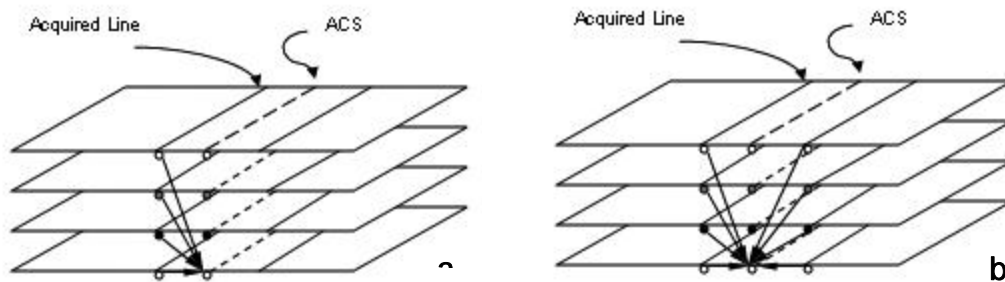


Figure 2-8 a : Use of ACS lines in VD-AUTO-SMASH b: Use of ACS lines in GRAPPA

2.7. GeneRalized Autocalibrating Partially Parallel Acquisitions (GRAPPA)

The only regenerative k-space technique commercially available at the moment is GRAPPA. The reason for offering two different parallel MRI methods is that there are a number of clinical applications in which the use of GRAPPA is advantageous. Examples include lung and abdominal MRI, real-time imaging, and the application for single-shot techniques. Parallel imaging with GRAPPA is particularly beneficial in areas where accurate coil sensitivity maps may be difficult to obtain. In inhomogeneous regions with low spin density such as the lung and the abdomen, it can be difficult to determine precise spatial coil sensitivity information. In these regions, the image quality of SENSE reconstructions might therefore suffer from inaccurate sensitivity maps.

In contrast, the GRAPPA algorithm provides good quality image reconstructions, since the sensitivity information is extracted from the k-space. In GRAPPA, central k-space lines are fit to calculate the reconstruction parameters.

This fitting procedure involves global information and is therefore not affected by localized inhomogeneities. The use of lines near the center of k-space also ensures that there is sufficient information to achieve a good reconstruction quality.

GRAPPA represents a more generalized implementation of the VD-AUTO-SMASH approach. Although both techniques share the same acquisition scheme, they differ significantly in the way reconstruction of missing k-space lines is performed. One basic difference is that the component coil signals $S_k(y)$ are fit to just a single component coil

ACS signal $S_l^{ACS}(k_y + m\Delta k_y)$, not a composite signal, thereby deriving the linear weights to reconstruct missing k-space lines of each component coil:

$$S_l^{ACS}(k_y + m\Delta k_y) \cong \sum_{k=1}^N n_k^{(m)} S_k(k_y). \quad (2.15)$$

This procedure needs to be repeated for every component coil, and since the coil sensitivities change also along read direction, the weights for the GRAPPA reconstruction are normally determined at multiple positions along read direction. After Fourier transformation, uncombined images for each single coil in the receiver array are obtained. Furthermore, unlike VD-AUTO-SMASH, GRAPPA uses multiple k-space lines from all coils to fit one single coil ACS line, resulting in a further increased accuracy of the fit procedure (i.e. over determined system) and therefore in better artifact suppression. A schematic description of an $R = 2$ VD-AUTO-SMASH and GRAPPA reconstruction procedure is given in Fig. 2.9.

The GRAPPA reconstruction formalism can also be written in matrix form. The vector \vec{S} represents the collected signal in each element coil at some position k and therefore has length N_c . Using GRAPPA in its simplest form, a set of weights $\hat{n}^{(m)}$ can be derived by fitting the signal \vec{S} to the ACS at the position $k + m\Delta k$ in each coil. Therefore, the coil weighting matrix $\hat{n}^{(m)}$ has the dimension $N_c \times N_c$ and may shift the k-space data in each coil by $m\Delta k$.

$$\vec{S}^{(m)} = \hat{n}^{(m)} \vec{S} . \quad (2.16)$$

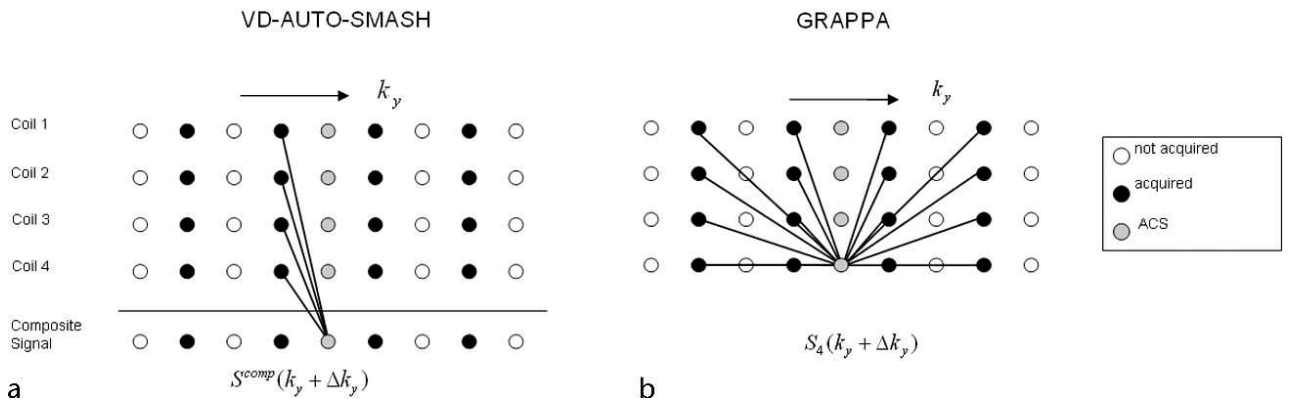


Figure 2.9 Schematic description of an accelerated ($R = 2$). **a:** AUTOSMASH and VD-AUTO-SMASH reconstruction process. Each dot represents a line in k-space in a single coil of the receiver array. A single line from all coils is fit to a single ACS line in a sum-like composite k-space. **b:** GRAPPA uses multiple lines from all coils to fit one line in one coil (here coil 4). This procedure needs to be repeated for every coil, resulting in uncombined coil images, which can be finally combined using a sum of squares reconstruction.

In contrast to a SMASH or VD-AUTO-SMASH complex sum image reconstruction, the GRAPPA algorithm results in uncombined single coil images, which can be combined using a magnitude reconstruction procedure (e.g. sum of squares). This provides a significantly improved SNR performance, especially at low reduction factors. Furthermore, signal losses due to phase cancellations are essentially eliminated using a magnitude reconstruction procedure.

Thus, previous drawbacks on k-space-based techniques, namely, phase cancellation problems, low SNR, and poor reconstruction quality due to a suboptimal fit procedure, are essentially eliminated. Furthermore, similar to SENSE, the GRAPPA algorithm works with essentially arbitrary coil configurations. Finally, as an additional benefit, ACS lines used to derive the reconstruction coefficients can in many cases be integrated into the final image reconstruction, in the same manner as intended in VD AUTO-SMASH [7].

The block wise reconstruction given above has been implemented using a sliding block approach. This uses the fact that each un-acquired line can be reconstructed in several different ways in a block wise reconstruction, instead of the only one combination possible in a strictly VD-AUTO-SMASH acquisition. For example, when using four blocks for the reconstruction (i.e., four acquired lines used to reconstruct each missing line), there are four possible reconstructions for each un-acquired line, two of which are shown in Figure 2-10. In GRAPPA, each possible reconstruction is performed for each un-acquired line, resulting in multiple possible reconstructions for each line. These lines are then combined in a weighted average to form the final reconstructed line, providing a robust reconstruction of each missing line. For perspective, it should be noted that this sliding block reconstruction is essentially reduced to the VD-AUTO-SMASH approach whenever the number of blocks is reduced to one [13].

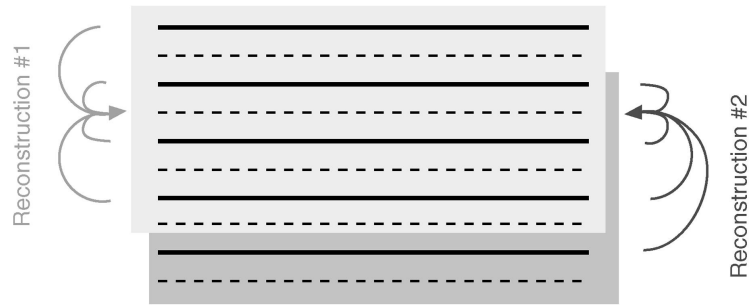


Figure 2.10 in a sliding block reconstruction, more than one reconstruction is possible for each missing line. Two of the four possible reconstructions for this missing line are shown.

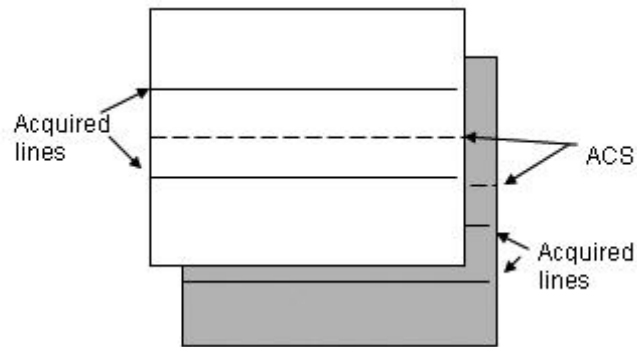


Figure 2.11 Sliding blocks in GRAPPA

GRAPPA in its basic form is VD-AUTO-SMASH. It can be extended to reconstruct the image in different ways by using different acquired lines to generate the same ACS lines. In this case, SNR is calculated for every image and the weighting coefficients are weighted according to the SNR obtained. This approach is called the sliding block approach Fig.2.11.

2.8 . SPACE RIP

SPACE RIP is a hybrid reconstruction method that first takes an inverse FFT along the frequency encoding making the rows/columns along the phase encoding direction, independent of each other. For every column, the k -space data is a FFT weighted by the coil sensitivity matrix. The data obtained for every coil can be written as (modified form [14]):

$$S_k(G_y^g, x) = \sum_{n=1}^N p(x, n) W_k(x, n) e^{i\gamma(G_y^g n x)}, \quad (2.17)$$

Where $W_k(x, n)$ is the complex sensitivity profile of the k th receiver array element. This expression is converted into matrix from combining the k -space data of all coils and then solved to obtain the required image.

If there are M coils and N lines are acquired per coil then, to generate one column of the image, a size $(M \times N) \times P$ matrix has to be inverted, making the reconstruction cumbersome. P is the number of total phase encodings in case of a full FOV scan. But this method is not restricted by the coil configuration of the k -space sampling. Matrix size reduces as reduction factor increases and reconstruction becomes faster unlike other methods where reconstruction time increases according to the acceleration.

The above expression can be converted to matrix form for each position x along the horizontal direction of the image, as follows:

$$\begin{bmatrix} S_1(G_y^1, x) \\ \cdot \\ S_1(G_y^F, x) \\ S_2(G_y^1, x) \\ \cdot \\ S_2(G_y^F, x) \\ \cdot \\ \cdot \\ S_k(G_y^1, x) \\ \cdot \\ S_k(G_y^F, x) \end{bmatrix} = \begin{bmatrix} W_1(x,1)e^{i\gamma(G_y^1 1\tau)} & \dots & W_1(x, N)e^{i\gamma(G_y^1 N\tau)} \\ \cdot & \dots & \cdot \\ W_1(x,1)e^{i\gamma(G_y^F 1\tau)} & \dots & W_1(x, N)e^{i\gamma(G_y^F N\tau)} \\ W_2(x,1)e^{i\gamma(G_y^1 1\tau)} & \dots & W_2(x, N)e^{i\gamma(G_y^1 N\tau)} \\ \cdot & \dots & \cdot \\ W_2(x,1)e^{i\gamma(G_y^F 1\tau)} & \dots & W_2(x, N)e^{i\gamma(G_y^F N\tau)} \\ \cdot & \dots & \cdot \\ \cdot & \dots & \cdot \\ W_K(x,1)e^{i\gamma(G_y^1 1\tau)} & \dots & W_K(x, N)e^{i\gamma(G_y^1 N\tau)} \\ \cdot & \dots & \cdot \\ W_K(x,1)e^{i\gamma(G_y^F 1\tau)} & \dots & W_K(x, N)e^{i\gamma(G_y^F N\tau)} \end{bmatrix} \times \begin{bmatrix} p(x,1) \\ p(x,2) \\ p(x,3) \\ \cdot \\ \cdot \\ \cdot \\ p(x, N) \end{bmatrix}, \quad (2.18)$$

Where F is the number of phase encodes used in the experiment, and K is the number of coils. Eq.2.18 is a matrix equation where the term on the left side of the equality is a $K \times F$ element vector containing the F phase encoded values for all K coils. The term on the far right is an N -element vector representing the “image” for one column. The middle term in Eq 2.18 is a matrix with $K \times F$ rows and N columns which are constructed based on the sensitivity profiles and phase encodes used. Hence, this approach is not restricted to the case where $K \times F \times N$. Solving Eq.3.18 for each position along the x axis yields a column by column reconstruction of the image.

Fig. 2.12 shows a schematic representation of the reconstruction process. As described above, each column in the image is reconstructed separately. In the case where the image

matrix has N rows and M columns, a block of M matrices must be inverted to reconstruct the M columns of the image. The matrices are not necessarily square, so that a pseudo inverse must be computed for each column. The choice of the number of phase encodes F affects the quality of the reconstruction. Increasing F results in an increase of the rank of the matrices, yielding pseudo inverses that are better conditioned. There is a large computation load associated with this reconstruction; however, the potential for parallelization is obvious, since each column can be reconstructed separately. For each slice, the pseudo inverses have to be computed only once. Subsequent updates of the same slice can be reconstructed by simple matrix vector multiplication, reducing reconstruction times to real-time rates [14].

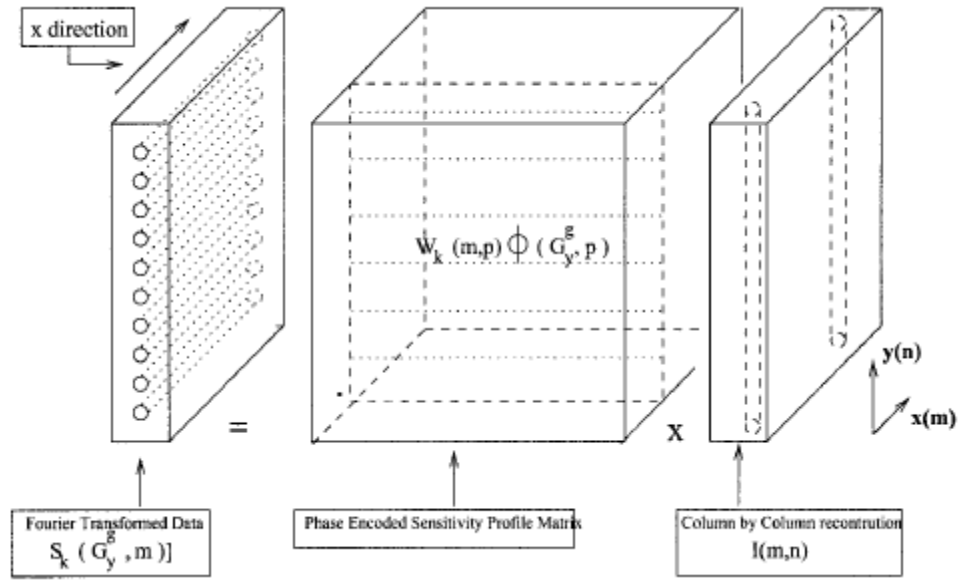


Figure 2.12 Schematic representation of the parallel reconstruction scheme. The matrix to the left represents the 1DFT of the chosen k -space data, the block of matrices in the center is the 3D sensitivity array formed by stacking M 2D matrices such as the one expressed in Equation (3.18). The matrix on the right represents the image, which is reconstructed column by column by inverting each matrix in the sensitivity array [14].

CHAPTER 3

Improved image reconstruction in parallel imaging using a uniform sensitivity coil

In this chapter we introduce a novel method for data acquisition and image reconstruction method for parallel magnetic resonance imaging (MRI). The proposed method improves the GRAPPA (Generalized Auto-calibrating Partially Parallel Acquisitions) method by simultaneously collecting data using the body coil in addition to localized surface coils. The body coil data is included in the GRAPPA reconstruction as an additional coil. The reconstructed body coil image shows greater uniformity over the field of view than the conventional sum-of-squares reconstruction that is conventionally used with GRAPPA. The body coil image can also be used to correct for spatial in homogeneity in the sum-of-squares image. The proposed method is tested using numerical and real MRI phantom data.

3.1 Introduction

Parallel magnetic resonance imaging (MRI) increases image acquisition speed by taking advantage of multiple surface radio-frequency (RF) coils [6, 7]. In conventional MRI, the full k-space data required for a certain field of view (FOV) and resolution are collected, whereas in parallel imaging the k-space is subsampled by a certain factor R . Consequently, individual aliased images are obtained for every coil. These images are either unfolded in the image domain to yield the final image or the missed k-space lines are reconstructed using a priori information from the spatially varying coil sensitivities.

The quality of the image reconstructed is an essential criterion for the success of parallel imaging. Many parallel imaging reconstruction techniques have been proposed. Examples include SENSE, SMASH, GRAPPA and their derivations [8, 10, 13, 14]. These methods can be divided into image domain and k-space methods. The k-space methods when used with the additional acquired auto-calibration data are very powerful in cases where determination of the coil sensitivity is difficult or is time varying. Among all these reconstruction methods, GRAPPA (Generalized Auto calibrating Partially Parallel Acquisitions) has been of most interest due to the improved performance in reconstructing high resolution images and overcoming the limitations in previous techniques like SMASH and VD-Auto-SMASH [5-8]. GRAPPA represents a more generalized implementation of

the VD-AUTO-SMASH approach [12]. Although both techniques share the same acquisition scheme, they differ significantly in the way reconstruction of missing k-space lines is performed. One basic difference is that the component coil signals are fit to just a single component coil auto-calibration signal (ACS), not a composite signal, thereby deriving the linear weights to reconstruct missing k-space lines of each component coil. This process is shown in Fig. 3.1 Data acquired in each coil of the array (black circles) are fit to the ACS line (gray circles). However, as can be seen, data from multiple lines from all coils are used to fit an ACS line in a single coil, in this case an ACS line from coil 4. The fit gives the weights which can then be used to generate the missing lines from that coil. Once all of the lines are reconstructed for all coils, a Fourier transform can be used to generate individual coil images. The full set of images can then be combined using a normal sum of squares (SoS) reconstruction.

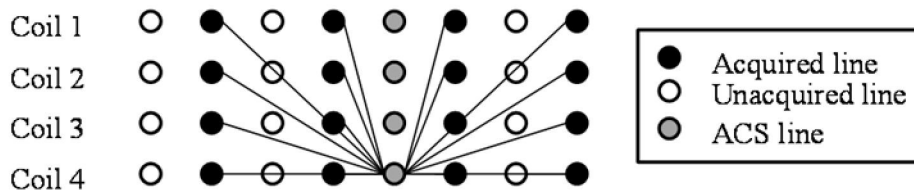


Figure 3.1 Schematic description of GRAPPA with an acceleration factor $R = 2$.

Reconstructing data in coil j at a line $(k_y - m\Delta k_y)$ offset from the normally acquired data using a block-wise reconstruction can be represented by:

$$S_j(k_y - m\Delta k_y) = \sum_{l=1}^N \sum_{b=0}^{N_b-1} n(j,b,l,m) S_l(k_y - bR\Delta k_y) \quad (3.1)$$

Where $S_j(k_y)$ is the signal in coil j at line k_y . In this case, N_b lines which are separated by $R\Delta k_y$ are combined using the weights $n(j,b,l,m)$ to form each line, corresponding to a reduction factor R . The coefficients $n(j,b,l,m)$ represent the weights used in this linear combination, the index l counts through the Individual coils, while the index b counts through the individual reconstruction blocks. This process is repeated for each coil in the array, resulting in L uncombined coil images which can then be combined using a conventional sum of squares reconstruction or any other optimum array combination [13]. In spite the success of the GRAPPA technique, the sum of squares step carried on as the final step of reconstruction can not guarantee uniformity over the field of view. In general, accurate knowledge of the coil sensitivity is required in order to produce uniform-intensity images. In this chapter we present an acquisition and reconstruction scheme that substantially improves the current GRAPPA reconstruction technique by utilizing the additional data collected from the uniform body coil.

3.2 Method

Simultaneous acquisition of reduced k-space data sets from both the body coil and the surface coil array is proposed so that a uniformly-weighted image reconstruction can be achieved. The additional body coil is included in the GRAPPA reconstruction process as a

regular surface coil, except that this special coil has the special property of uniform sensitivity over the FOV. This approach is illustrated in Fig. 3.2B. The process of individual coil estimation is carried on using GRAPPA according to [13]. After the reconstruction of every coil image, the body coil image among all images has uniform sensitivity and can be regarded as the final reconstruction R1 in Fig. 3.3. Unfortunately, this body coil image may suffer from lower SNR because the coil is far away from the imaging volume. It may also suffer from reconstruction artifacts during GRAPPA reconstruction for the same reason. Therefore, the sum-of-squares reconstruction of all images generated from GRAPPA could be more interesting since the resulting image will have better SNR, lower artifact level and better uniformity R2 in Fig. 3.3. Alternatively, a sum-of-squares reconstruction of only the surface coils can be compensated for non-uniformity by a pixel by pixel comparison to the body coil image to assure a uniform sensitivities distribution in the final image R3 in Fig. 3.3. A procedure for intensity correction is shown in Fig. 3.4 where the ratio of smoothed versions of the body coil image and the GRAPPA image are fitted to a low-order polynomial to get the intensity correction function.

Simulation is performed using the numerical Shepp-Logan (SL) phantom [16] and 6 surface coils profiles calculated using the Biot-Savart law for circular loop coils. A 128x128 SL image is multiplied with the sensitivity of the 6 coils; Fourier transformed (FT) to obtain a set of six full k-space data sets. A seventh data set is obtained by taking the FT of the SL image directly to simulate a body coil acquisition. The seven data sets are then subsampled with a factor of $R = 2$. A set of 32 lines at the center of k-space is also retained

for GRAPPA training to determine the filter coefficients. Image reconstruction is performed as described above. For comparison, conventional GRAPPA reconstruction is applied to the six surface coils and sum-of-squares is used in the final reconstruction.

The described reconstruction steps are applied to a real MR phantom acquired with a gradient echo sequence on a Philips 3T Achieva system. Because the system does not allow simultaneous receive of signals from the surface coil array and the body coil, two experiments are performed sequentially using the cardiac coil array with six elements and the body coil. The scan parameters are TR/TE = 11/2.7 ms, FOV = 40x40 cm, slice thickness = 5 mm, matrix size = 448x448.

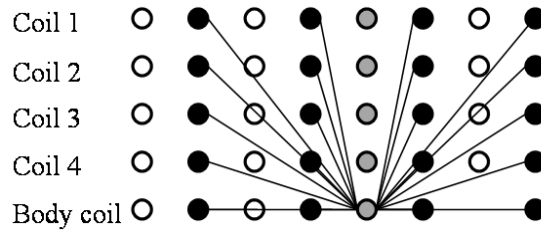


Figure 3. 2. GRAPPA reconstruction with the additional body coil.

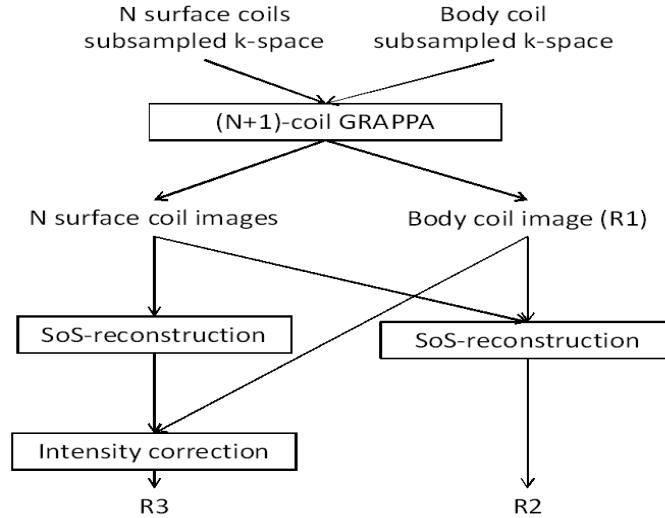


Figure 3. 3 The modified reconstruction method with the body coil. Possible reconstruction options are marked with R1, R2, and R3.

3.3 Results

Fig. 3.5 shows the results of applying the new method to the simulated SL data. The conventional GRAPPA image Fig. 3.5A shows noticeable intensity non uniformity, especially when compared to the body coil image reconstructed using the proposed method Fig. 3.5 B. The intensity correction obtained by dividing smoothed version of both images is shown in Fig 3.5C. The corrected image obtained by multiplying the images in (A) and (C) is shown in Fig 3.5D where better uniformity is evident, although some blurring of edges is noticed. The results of applying the proposed method to the real MR phantom are shown in Fig. 3.6. The GRAPPA-reconstructed body coil image Fig.3.6B shows excellent

uniformity but lower SNR than the GRAPPA sum-of-squares image Fig. 3.6A. The body coil image shows some residual artifact from GRAPPA that could be due to the lower SNR and the higher g-factor [14] in the middle of the image. The intensity-corrected image is shown in Fig. 3.6D using the correction in Fig. 3.6C.

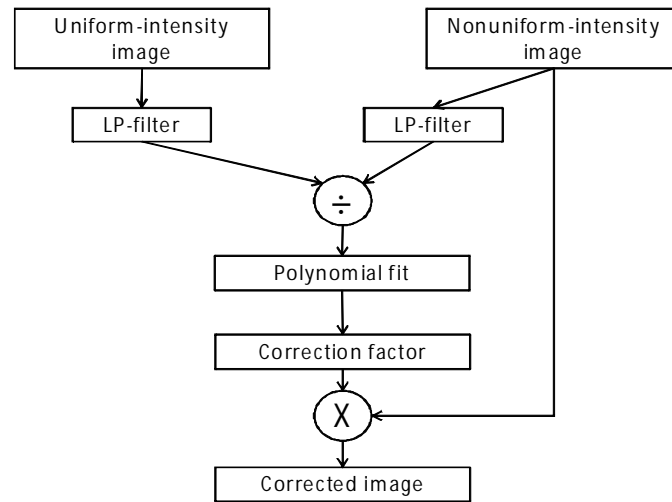


Figure 3.4 A procedure for intensity correction using the uniform intensity image. LP-filter is low-pass filter.

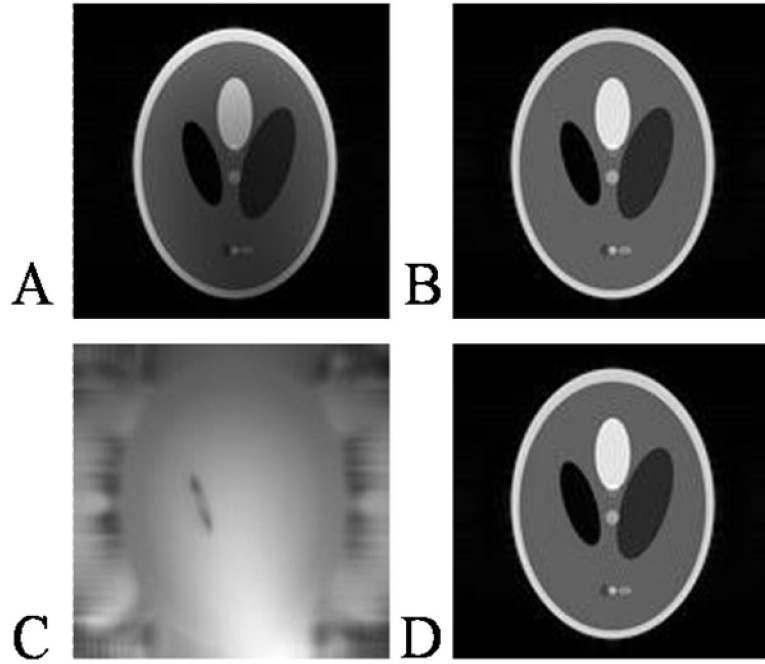


Figure 3.5(A) the sum-of-squares reconstruction of GRAPPA. (B) The body coil image using GRAPPA reconstruction. (C) The correction function obtained by dividing smoothed versions of (A) and (B). (D) The intensity-corrected sum-of-squares image.

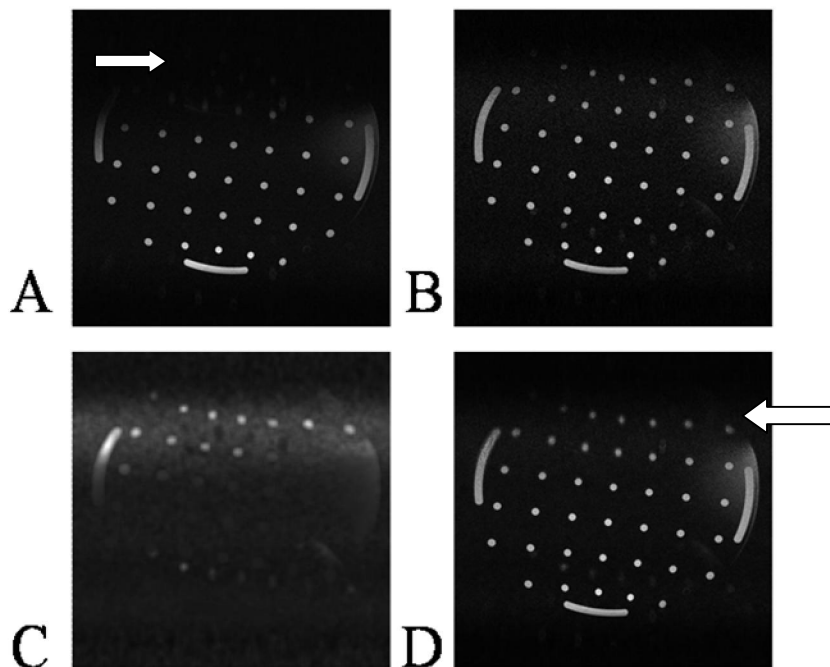


Figure 3.6 (A) The sum-of-squares reconstruction of GRAPPA. (B) The body coil image using GRAPPA reconstruction. (C) The correction function obtained by dividing smoothed versions of (A) and (B). (D) The intensity-corrected image.

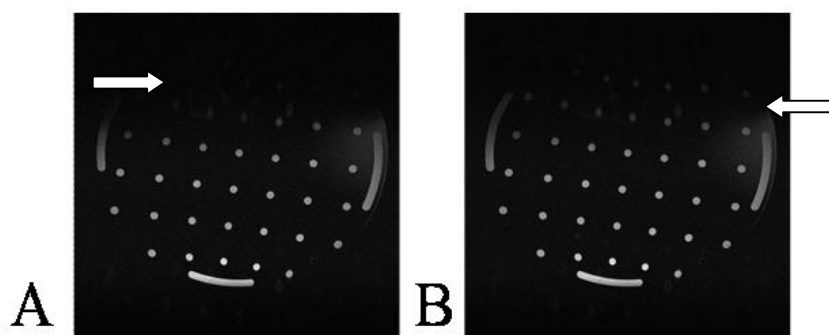


Figure 3.7 (A) the sum-of-squares reconstruction of GRAPPA using only surface coils. (B) The sum-of-squares reconstruction of GRAPPA using both the surface coils and the body coil.

3.4 Discussion

The SL results in Fig. 3.5 shows that uniform intensity in the final image is possible if a body coil is incorporated in the acquisition and reconstruction phases of a parallel imaging pipeline. In spite the high SNR of the reconstructed images using the local surface coils compared to the SNR of the body coil, the reconstructed image of the body coil show some areas that are not seen before using the local coil alone as shown by arrow in fig.3.6B, moreover the reconstructed image of the body coil show uniform sensitivity over the entire field of view, compared to the individual reconstructed images of the local array coils which is sensitive according to its geometry and its location to the field of view. Nevertheless, the uniformity of the body coil image may be in specific situations very important like in phase contrast [17] or strain encoded MRI [18].

The acquired data by the body coil is considered an additional data set added to the local surface coils. The benefits of these data of the body coil not restricted to improve the final reconstructed image phase only but it can be extended to improve in the final image details compared to the conventional GRAPPA. As by applying other reconstruction criteria can with the body coil data as shown in fig .3.3.

In reconstruction criteria of R2 where the body coil used with the local coil to get sum of square image as conventional GRAPPA, so in spite the final image will suffer from the lack

of phase information but, it show improvement over the final image of the conventional GRAPPA with the local surface coils only as shown by arrow in fig 3.7B with real phantom data. Where some area in fig 3.7A using only the local surface coils are not clear or even shoed at all specially in the edges of the image compared to the same areas using both body coil data and local surface coil.

So, the intensity correction is also possible using the body coil image. Similar results are obtained for real MR scan of a physical phantom in spite the current limitations of MR hardware where no Simultaneous acquisition between the main body coil and the local surface coil array can be implemented. A small residual artifact is noticed in the GRAPPA-reconstructed body coil image. This artifact may be due to the high g-factor in the middle of the image that manifest the lower SNR of the body coil signal where is the filling factor of the main body if low due to the far distance between main body coil and the object to be imaged.

The benefit of the uniformity of the body coil and the high SNR of localized surface coils can be traded off in a sum-of-squares reconstruction of the whole coil data as shown in Fig. 3.7. However, may be an image processing techniques can be used to overcome the residual artifact in the final reconstructed image. Also, a new methodology of the final reconstruction or the intensity correction can be used in a pixel level by trying to keep the level of high SNR of the local array and use the phase information from the main body coil in away that decrease the noise contribution from the body coil data.

Also, the benefits of the body coil can be extended to another parallel imaging methods like Auto-SENSE [17], where the parallel imaging reconstruction applied onto the image domain compared to the application we used here with GRAPPA into the k-space domain. Here with Auto-SENSE the central band lines to estimate the sensitivity of each coil without need for a separate scan.

So, by using the body coil uniform sensitivity it may improve the phase of the final reconstructed image, a preliminary tested results can show an improvement of the final image phase over the ordinary Auto-SENSE.

3.5 Conclusion

We proposed a new method for parallel imaging acquisition and reconstruction that improves the current GRAPPA technique in terms of image uniformity over the entire FOV. By overcoming the current hardware limitation in MRI systems for simultaneous acquisition, the proposed method will enable improved image quality in MRI parallel imaging. The new method can provide a way to improve the final reconstructed image phase, where it is essential point in different MR applications. Overcoming the noise attributed by the body coil, may reduce the current apparent artifacts into the final reconstructed image and considered.

CHAPTER 4

Optimizing kernel size in generalized auto-calibrating partially parallel acquisition in parallel magnetic resonance imaging

In this chapter we will show that a variable kernel with a size dependent on the coil sensitivity used in GRAPPA algorithm can lead to better image quality instead of using fixed in size for all coils. The kernel size is estimated from the ratio of the coil sensitivities obtained from a reference scan or from the same dataset. Conventional GRAPPA kernel estimation and image reconstruction is modified to employ the variable-size kernel for improved reconstruction.

4.1. Introduction

Parallel magnetic resonance imaging (MRI) is a family of acquisition and reconstruction techniques that increase image acquisition speed by taking advantage of the localized sensitivity of multiple surface radio-frequency (RF) coils [17]. In MRI, the image is reconstructed from a set of samples collected in the spatial frequency domain, also known as k-space. In conventional (un-accelerated) MRI, the full data in k-space are collected corresponding to a certain field of view (FOV) and resolution in the image, whereas in parallel imaging the k-space is subsampled by a factor R . Consequently, individual aliased images are obtained for every coil. These images are either unfolded in the image domain, or the missed k-space lines are estimated from the acquired data and prior information about the coil sensitivities. Many parallel imaging reconstruction techniques have been proposed like sensitivity encoding (SENSE), simultaneous acquisition of spatial harmonics (SMASH), generalized auto-calibrating partially parallel acquisition (GRAPPA) and their derivatives [13]. These methods can be generally divided into k-space methods and image domain methods. The k-space methods when used with the additional acquired auto-calibration data are very powerful in cases where determination of the coil sensitivity is difficult or is time varying.

In GRAPPA, reconstruction of data in coil j at a line $(k_y - m\Delta k_y)$ offset from the acquired

data is given by:

$$S_j(k_y - m\Delta k_y) = \sum_{l=1}^N \sum_{b=0}^{N_b-1} n(j,b,l,m) S_l(k_y - bR\Delta k_y) \quad (4.1)$$

Where $S_j(k_y)$ is the signal in coil j at line k_y . In this case, N_b lines which are separated by $R\Delta k_y$ are combined using the weights $n(j,b,l,m)$ to form each line, corresponding to an under-sampling (or reduction) factor R . The coefficients $n(j,b,l,m)$ represent the weights used in this linear combination. The index l counts through the individual coils, while the index b counts through the individual reconstruction blocks. This process as shown in Fig.4.1 is repeated for each coil in the array, resulting in L un-combined coil images which can then be combined using a conventional sum of squares reconstruction or any other optimum array combination [9].

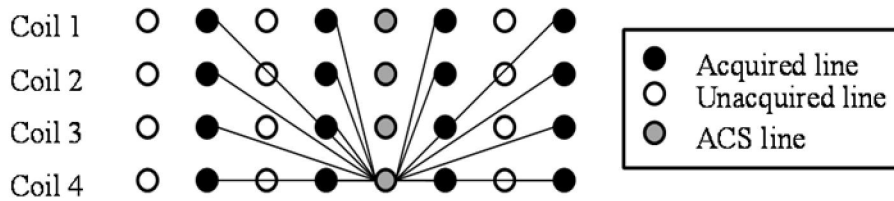


Figure 4.1. Schematic description of GRAPPA with an acceleration factor $R = 2$ and a single auto-calibrating line.

The interpolation kernel is usually small but fixed in size for all coils. In this work, a general variable-size kernel approach is introduced that derives from the theory introduced by Bao and Maudsley [19]. The variable kernel used in this work is two-dimensional (2D) with coil-dependent size. The kernel size is estimated from the coil sensitivities obtained from a reference scan or from the same dataset. Conventional GRAPPA kernel estimation and image reconstruction is modified to employ the variable-size kernel for improving the reconstruction.

4.2. METHODE

The MR signal generated in the l th coil is given by

$$d_l(k_x, k_y) = \sum_{x=0}^{N_x-1} \sum_{y=0}^{N_y-1} r(x, y) C_l(x, y) \exp(-j2\pi(xk_x + yk_y)) \quad (4.2)$$

Where r is the weighted spin density of the imaged object and C_l is the coil sensitivity of coil l .

Following the work in [10], Eq. 4.2 can be re-written as

$$d_l(k_x, k_y) = \sum_{x=0}^{N_x-1} \sum_{y=0}^{N_y-1} r(x, y) C_l'(x, y) \frac{C_l(x, y)}{C_l'(x, y)} \exp(-2j\pi(xk_x + yk_y)) \quad (4.3)$$

Where C_l' is the sensitivity map of coil l . Following the convolution theorem

$$d_l(k_x, k_y) = \sum_{\omega_x} \sum_{\omega_y} d_{l'}(\omega_x, \omega_y) \tilde{C}_{l,l'}(k_x - \omega_x, k_y - \omega_y) \quad (4.4)$$

Where

$$\tilde{C}_{l,l'}(k_x, k_y) = FT \left\{ \frac{C_l(x, y)}{C_{l'}(x, y)} \right\} \quad (4.5)$$

and $FT\{\cdot\}$ denotes the Fourier transformation. Eq. 4.5 shows that the relation between the signals in any two coils is a convolution operation wherein the convolution kernel is the Fourier transform of the ratio between the sensitivity maps of these two coils. The optimal convolution kernel is thus specific to each coil pair and will be different in size and shape depending on the relative coil sensitivities and the geometry of the coil array. The estimation of the missing lines of each of the coils in conventional GRAPPA is given by,

$$d_{l'}(k_y - m\Delta k_y, x) \approx \sum_{l=1}^L \left[\sum_{b=0}^{N_b-1} n(l', b, l, m) d_l(k_y - bR\Delta k_y, x) \right] \quad (4.6)$$

Although the theoretical kernel n is of infinite extent, its energy is concentrated at the origin. This is because the individual coil sensitivity profiles are inherently smooth and the Fourier transform of this smooth sensitivity ratio is concentrated in the center of k -space as shown in Fig. 4.3. This provides a justification for the small size of the convolution kernel used in GRAPPA reconstruction.

Here, we extend the GRAPPA method to include the concept of coil-specific convolution kernel by allowing the size of the kernel n to vary as a function of the two coils l and l' . Fig.4.2 shows the size of the function when truncated at 90% of its total energy (white rectangles). The conventional GRAPPA method is modified to use this truncation window size as the kernel size for each pair of coils.

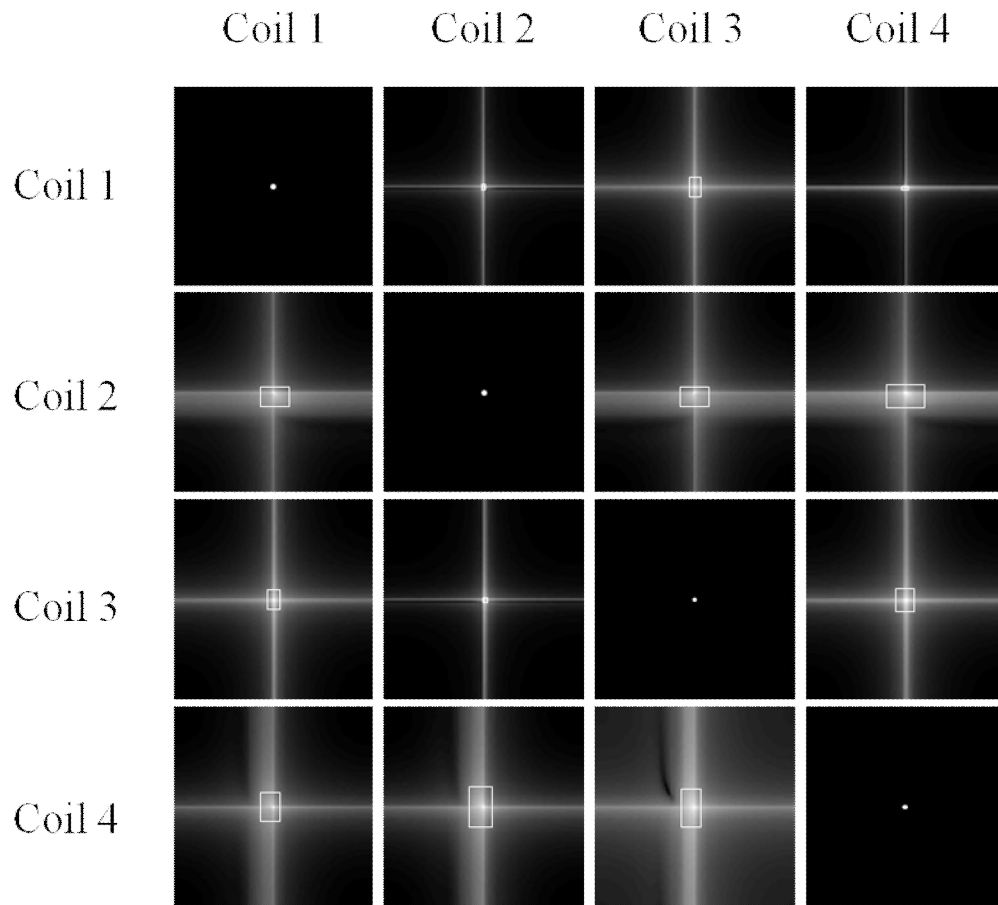


Figure 4.2. The magnitudes of the Fourier transform of the ratio between the sensitivity of coils pairs in a four-coil array using the Shepp-Logan phantom. Brightness is in logarithmic scale for better visualization. The rectangular boxes overlaid correspond to truncation

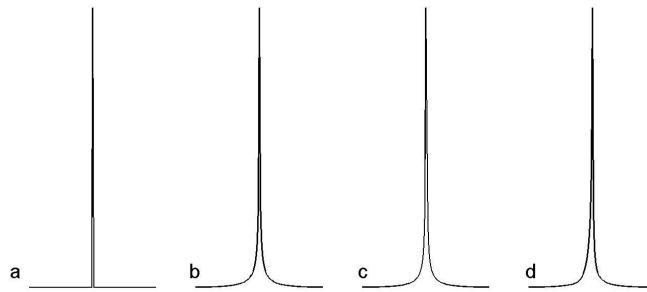


Figure 4.3. Profiles through the center of the Fourier transform of the coil sensitivity ratios between the four coils and the first coil. Note the narrow width of these profiles.

The proposed technique is validated using simulated data of the Shepp-Logan (SL) phantom [16] with a matrix size 128x128. The phase encoding direction is left-right. Eight loop coils are used in the simulation with coil sensitivity derived from the Biot-Savart law for circular loop coils. Complex Gaussian noise is added to the simulated data of all coils with zero mean and standard deviation that is 0.001 times the root-mean square value of all signals in the eight coils. Different reduction factor ($R=2, 3, 4$) were tested as well as different number of ACS lines (8, 12, 16 and 20 lines).

To determine the kernel size for each coil pair was truncated at 60% of its total energy. The size of the truncation window in the direction of phase encoding is divided by the reduction factor R to get the number of blocks or the kernel size to be used in GRAPPA reconstruction.

The kernel size in the frequency encoding direction is the same as the size of the truncation window in that direction. The kernel coefficient estimation is performed by stacking the

ACS data from all coils and then using regularized inversion of the resulting linear system to get the different kernels.

These kernels are then used in the reconstruction as in GRAPPA except that each kernel corresponding to a coil-pair has its own size. The reconstruction quality is quantified by the SNR measured in the large grey ellipse to assess the noise amplification. The SNR also serves as a measure of the intensity of reconstruction artifacts.

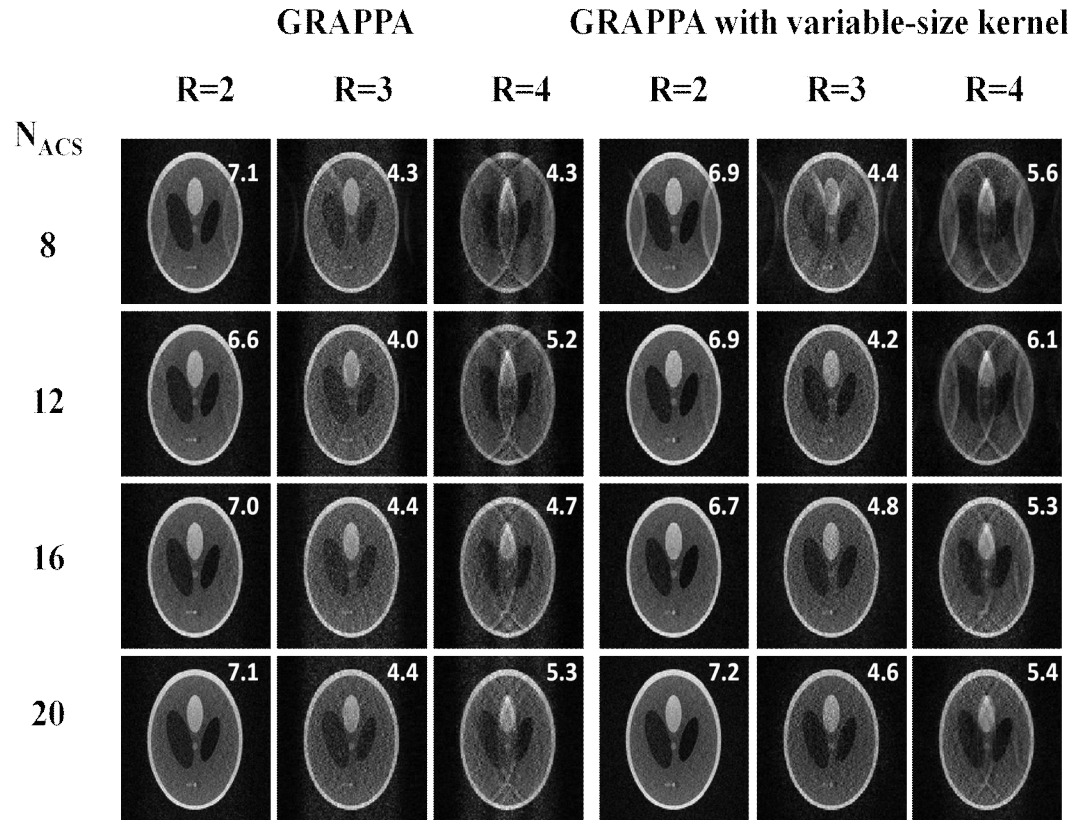


Figure 4.4 The reconstructed sum-of-squares images using GRAPPA and variable-size kernel GRAPPA for different number of ACS lines and different reduction factors R. The number overlaid on each image is the SNR calculated in a region of interest in the large grey ellipse.

4.3. RESULTS

The images reconstructed using the proposed variable-size kernel GRAPPA are shown in Fig. 4.4, along with the conventional GRAPPA reconstruction using a kernel size of four. Less artifacts and better SNR is noticed when the variable-size kernel is used than with the conventional fixed-size kernel when the number of ACS lines is sufficiently high.

The better performance of the proposed method is evident for different acceleration factors and for ACS lines greater than eight.

The performance with the variable-size kernel approach is less successful than GRAPPA when the number of ACS line is small. This is due to the ill-conditioning of the

System of equations used to estimate the kernel when the number of ACS lines is relatively small. However, for moderate or large number of ACS lines the performance of variable-size kernel is remarkable in suppressing noise that is otherwise amplified with the fixed-size kernel.

4.4. Discussion

The variable size convolution kernel is much more than an extension of the fixed-size kernel initially employed in GRAPPA. The variable size kernel follows directly from the mutual coil sensitivity of each coil pair. The kernel is defined by the ratio of the coil sensitivities which depends on the inherent sensitivity of each coil in addition to the geometry of the coil array and the locations of coils into the field of the view. The kernel is a 2D function and is concentrated in a direction that depends on the location of the two coils under consideration relative to each other.

In spite the success of the convential GRAPPA kernel, where a fixed size kernel is employed [13], the theoretical base of the GRAPPA was not clear upon it the criteria of choosing and optimizing the fixed size kernel can be clarified. This can be shown clearly when choosing the number of blocks needed for the reconstruction [13], where this number

was recommended to be in a range vary from two up to four, but without solid criteria for optimizing this number on theoretical base.

However in fig.4.2 the representation of the paired coil profiles show a different in size of the kernel, represented by the white rectangles, based on coil to coil profiles. As mainly the coils are sensitive to it is nearest areas within the field of the view , but this sensitivity are different form coil to coil based on the orientation of the sensitivity per each coils, some coils are sensitive to diagonal directions other horizontal. So, the paired correlation between coils profiles will vary accordingly. Mainly the GRAPPA technique build on using the own coil data and other coils data to reconstruct the missing and un-acquired lines with coil, the relation between the coil and other coils will clarify the contribution form other coils to this coils which basically will vary form coil to another.

In this work the kernel size was directly computed from a full-resolution coil sensitivity map, but it can be directly estimated from the auto-calibrating signal acquired in the same dataset. This approach is preferred to acquiring a full scan reference acquisition since it can avoid registration problems when patient motion occurs. Estimation of a low-resolution coil sensitivity ratio can then obtained in the same manner as in auto-calibrating SENSE methods.

The proposed approach of using variable-size kernel can improve our understanding of how GRAPPA works and can help in optimizing the reconstruction as well as the selection of various scan parameters like the number and locations of the ACS lines. Where mainly the ACS lines are located at the center of the k-space where the low frequency component

located with a high SNR. However, the outer lines at the edges of the k-space represent the high frequency components, so we can employ some ACS lines at both edges of the k-space to be used to reconstruct the outer lines of the k-space using the same concept of variable kernel size, and using the centralized ACS to reconstruct with the variable kernel size to reconstruct the main portion of the k-space with low frequency component and high signal to noise ratio.

Also the number of the ACS lines to be acquired to get the GRAPPA coefficients to reconstruct the missing data, as the ACS lines considered an additional amount of time to the scan time specially into the auto-calibration method, where the sensitivity of each coil estimated from a fully sampled central band within the k-space as in GRAPPA, we represent here by using the variable size kernel the result of combining different number of ACS at different reduction factor, where with high reduction factor and with the same number of ACS lines as fixed kernel, the variable size kernel represent high SNR into the final reconstructed image as shown in fig 4.4.

However the performance of the variable size kernel is get lower than fixed kernel where the number of the ACS decreased, so adapting and improving the performance of the variable size kernel to overcome the less performance than the fixed within small number of ACS considered potential point for more investigation, which will improve the acquisition time and final reconstructed image.

4.5. Conclusion

GRAPPA reconstruction with the proposed variable-size kernel provides better image quality with a reduction in the power of artifacts and enhanced SNR at high reduction factor. The variable-size reconstruction does not require the acquisition of additional data and can be implemented with little modification to the existing GRAPPA technique. The variable size kernel considered a base to understand the theoretical base of the GRAPPA technique used in the parallel imaging.

CHAPTER 5

Neural Network Based Gridding of non-Cartesian samples in multi-channel array acquisition

In this chapter will examine how Parallel Imaging can be used as tool to solve a classic imaging problem , the convolution Gridding , we introduce a new method that combine the benefits of parallel Imaging and Neural Network techniques in order to grid the non-Cartesian points into grid one and over come the current limitations of the current techniques.

5.1. Introduction

In spite the non Cartesian sampling showing a several advantage over the Cartesian from the efficiency of K-space coverage, reducing the inhomogeneity of the magnetic field and decreasing the acquisition time, which considered a major factor in different MRI applications where speed is concerned as in Cardiac Imaging and Breath-hold applications[17,20], it show some difficulty in the image reconstruction phase as many of the acquired data points didn't fall generally on a grid points where a direct Fourier transform will not be useful to get the final image. So, a step of *re-gridding* the acquired data to be fall into grid points is a must. Gridding is considered an old problem which initiated from different field of applications i.e. radar, Computed tomography and Magnetic Resonance.

The convolution gridding [21] which considered the golden standard method to transfer the non Cartesian point to Cartesian one before taking the direct Fourier transform. However, this method needs a DCF, Density Compensation Function, to assure a uniform sampling density all over the K-space.

This happened due to the nature of non uniform sampling where mainly a non-uniform density trajectory is employed. The computing of DCF for many trajectories such as rosette [23], or different trajectories [24, 25, 26] is not considered a trivial one like the radial trajectory or even like the spiral trajectory. Recently the parallel imaging can show an

additional method to be used in the convolution gridding (GROG). The parallel imaging trying to shift the acquired non-Cartesian points to the nearest missed Cartesian one using the spatial information from the array of coils and reconstruction algorithm like GRAPPA [13]. To perform this shift from one point in k-space to another one a weight set has to be computed either from a pre-scan or from the acquired data itself [27].

5.2. Method

The GRAPPA operator formalism can reformulate the GRAPPA reconstruction as a matrix operator, similar to ladder or propagator operators, that shifts data in K-space with a small amount.

$$s(k_x, k_y + n\Delta k_y) \approx G_n \cdot s(k_x, k_y), \quad (5.1)$$

Where $s(k_x + nk_y)$ is the acquired point, G_n are the appropriate coil weighting factors (weights) for the desired shift, and $s(k_x, k_y + n\Delta k_y)$ is the vector containing the signal from each receiver coil at the desired location. It is important to note that this formulation is equivalent to GRAPPA with a single source point and a single target point. The weight set is simply a square matrix of size $NC \times NC$, where NC is the number of coil elements used for the acquisition. Because this weight set is similar to a ladder or propagator operator in quantum mechanics, the term “GRAPPA operator” is used to describe it. The GRAPPA operator can be derived in the same fashion as standard GRAPPA weights.

Namely, a fit of points with the appropriate relationship is performed with the use of the pseudo inverse:

$$S_{ACS}(k_x, k_y + n\Delta k_y) \cdot \text{pinv}(S_{ACS}(k_x, k_y)) \approx G_n \quad (5.2)$$

In these equations, the signal matrices S_{ACS} are made up of a collection of signal vectors from an auto calibration dataset with adjacent distance relation-ship. eq 5.2 can show another important property of the GRAPPA operator that is a small shift operator G_n can be derived from an operator for a larger shift G_n by taking the nth root of the

Larger operator [27] as follows:

$$G_{\sigma} = G_{n.\sigma}^{1/n} \quad (5.3)$$

Where G_{σ} represents the base weight matrix which used to determine the weights needed to shift the non-Cartesian points to Cartesian one with arbitrary shifts along the orthogonal directions. This arbitrary shift needed to shift the non-Cartesian points to the nearest Cartesian one is calculated using the K-space trajectory as shown in fig .5.1. As the calibration set of weights in orthogonal direction can be performed once then any smaller shifts can be derived from a smaller one as follows:

$$s(k_x + \delta_x, k_y + \delta_z) = G_x \cdot s(k_x, k_y, k_z)$$

$$=G_{\sigma_x}.G_{\sigma_y}.G_{\sigma_z}.s(k_x,k_y,k_z) \quad (5.4)$$

From Eq 5.4 we can see that many non-Cartesian points can be mapped to the same Cartesian point so, a simple averaging will be needed to get the final value of the Cartesian point and the arbitrary shift does not imply to be restricted for an integer value.

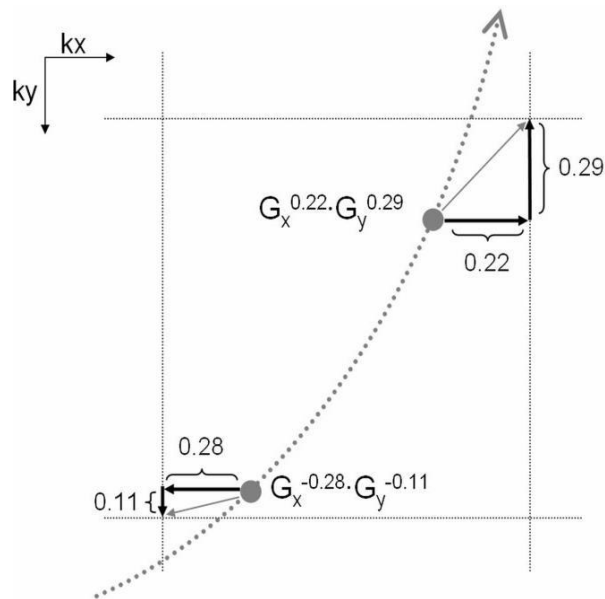


Figure 5.1. GROG gridding of non-Cartesian points. Cartesian destinations are at the intersections of the straight, finely dotted lines, and consecutive samples of an arbitrary trajectory are represented by solid circles. GROG grids a non-Cartesian data point by shifting it to its nearest Cartesian location via an appropriate weight set [27].

So, in order to employ GROG to grid the non-Cartesian points, a calibration signal must be used to determine the *base matrices weights* for steps in the G_x and G_y directions (for 2D imaging). For arbitrary k-space trajectories, this calibration signal can be a low-resolution Cartesian dataset with Nyquist sampled where steps of $\Delta k=1$ are performed (i.e., G_x is calculated from the points in the read direction, and G_y from the points along the phase encoding direction by fitting each point to the point adjacent to it in the appropriate direction Eq. 5.4 so the GROG base weight matrix can be calculated, then it can be used to calculate the weighted set for a smaller shifts.

The main advantage of GROG is that no pre-calculated DCFs or other parameters are required for gridding, whereas convolution gridding requires a DCF in addition to other parameters. While this is not a difficulty for the radial or spiral trajectory, the ability to grid BLADE, rosette, or stochastic data without having to calculate a DCF is highly advantageous. It is important to note that the effective DCF used in GROG, i.e., the averaging of shifted points that map to the same Cartesian location, cannot be used for other gridding techniques, because GROG explicitly calculates the values of the Cartesian points. Thus, after applying the appropriate GROG weights to each non-Cartesian point, the resulting dataset is made up of purely Cartesian points, which can simply be averaged.

It would also be possible to weight the shifted points with scaling factors that depend on the distances of their GROG shifts, although this method of calculating the DCF has not been

examined. In addition, for under sampled datasets, GROG automatically performs an approximation of the high SNR, low artifact energy DCF proposed by Pipe.[22] for under- sampled datasets. Thus, under sampled data are also correctly density-compensated without the need for considerations about the degree of under sampling present in the dataset.

5.3. GROG considerations

- **Data oversampling.**

However, the stability of the GROG technique may be affected by the presences of the noise especially with the dataset with low SNR [27] as it will affect the reconstructed image compared with the convential convolution gridding, thus to improve the performance of the GROG we need to oversampling the data along the read out directions , where the advantage of oversampling is to increase the number of non-Cartesian points which shifted and contributed to the same Cartesian point from the multi-channel array of coils, thus increasing the stability of the algorithm generally and specially in the noisy data sets. So, oversampling the data along the read out direction is considered an essential point in the GROG algorithm.

- **The measurement of the calibration data set.**

In order to use the GROG a calibration data set is needed to determine the base weight matrix, and hereby to estimate the values of G_x , G_y , with a constant distance between adjacent points. The calibration data ser takes the form of Cartesian data set with a

unity shift i.e. $k=1$, so the GROG weight can be estimated as GRAPPA coefficient. However, most of the non-Cartesian data sets don't imply to have enough and sufficient Cartesian data points to allow a direct estimation of the GROG weights using the GRAPPA operator. So, either a separate Cartesian data set has to be acquired prior the scan as in routine GROG, which may be affected by other factors as patient motion or changing the field of view, or using a self-calibration GROG [28] which is restricted to Cartesian trajectories with a predefined relationship between many pairs of values along the trajectory, as in radial or spiral trajectory, this also may be degraded by either the lack of instability of GROG weights estimation and reconstruction due to using of fewer data points for calibration or a more sophisticated algorithms [28].

The self-calibration algorithm used for GROG is built on the assumption that a matrices with a unity shifts in the logical directions are commute, as shifts in one orthogonal direction followed by shift in another orthogonal direction can be done in opposite order (self-grog ref) this assumption can not be always hold in practical (self-grog ref), so we can conclude that a trajectories with no Cartesian portion or radial symmetry the self-calibration GROG will not be beneficial and need for additional scan will be a must in order to use GROG in gridding reconstruction.

5.4. Using Neural Network for GROG base weight estimation

The Neural Network showed a great potential in different applications in different clinical fields. However, in this section we showed another potential for neural network in MRI applications. As previously illustrated the usage of GROG in gridding in spite the

current limitations in this techniques from the need of oversampling the data in the read out direction to assure stability of the algorithm or need for calibration data set. However, the neural network can be used as novel approach in gridding without the current limitations of GROG.

The idea is to use directly the acquired non uniform sampling data form the multi-channel array of coils directly, these data will be used as learning data set for a supervised neural network, where the input data is the acquired data form all coils and output data is the data per each coil, as shown in fig 5.2, where the NN will learn the proper weights to shift the non-uniform sample within the k-space to the nearest randomly set of acquired non-uniform samples using the spatial information from the coil itself and other coils in the array ,then the process will be repeated for each coil , so the weight set per each coil will be estimated.

Here the algorithm will be independent form the trajectories whatever it will be with Cartesian data set or non Cartesian one , also the algorithm so the algorithm will not need any calibration data set it considered as self-calibration method . After training the NN with the proper weights, then we can apply the acquired data form multi-channel array to the trained neural network to reconstruct the Cartesian points directly with tow different strategies in wither we can use single source to single target approach, Where the source point will be the non-Cartesian point and the target one will be the nearest Cartesian point or we can use multi-source point.

This will be the non Cartesian point form the acquired data to single target point which will be nearest Cartesian point. As the idea here is that any non-Cartesian point will be surrounded by four Cartesian points. In this way we can reverse the relation to estimate the Cartesian point directly.

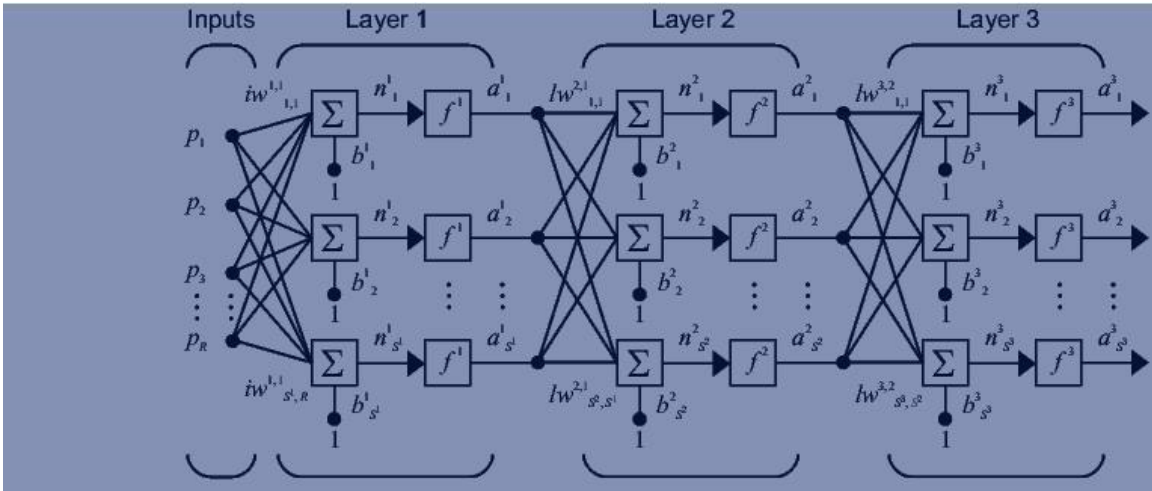


Figure 5.2. The architecture of supervised back propagated Neural Network

The algorithm can be summarized as follows

- Acquired the data of multi-channel array of coils with non Cartesian sampling scheme.
- Apply ALL acquired data to a supervised NN for training

- Every non Cartesian point will be used as input and the output will be the nearest surrounding non-uniform samples with a distance ≤ 1 this will be repeated per each coil within the array
- Reconstruct the Cartesian data per each coil used trained NN and weights

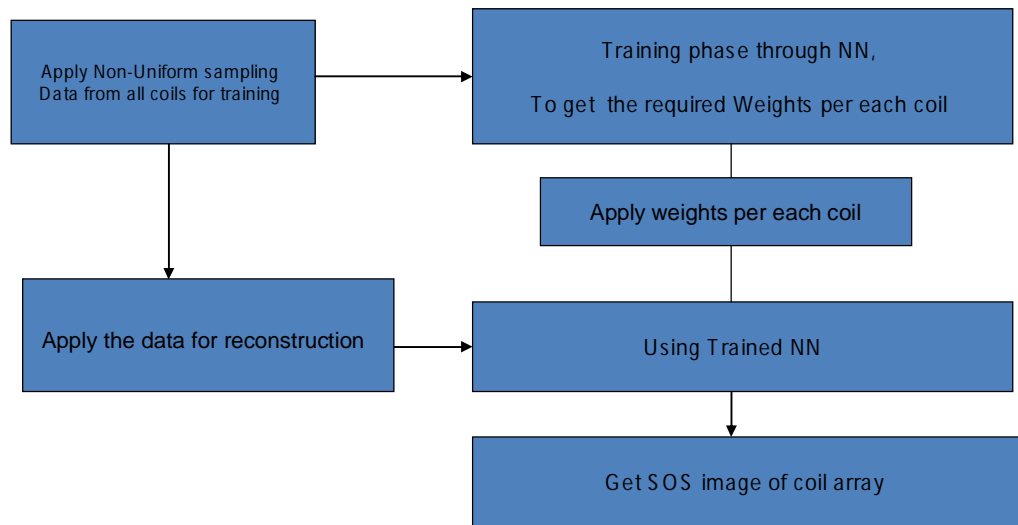


Figure 5.3. The proposed Neural Network algorithm for estimating the Cartesian data points from non Cartesian data

5.5. Experiment

The proposed technique is validated using simulated data and real data, the simulated data of the Shepp-Logan (SL) phantom [16] with a matrix width of 128 for a radial trajectory and Spiral trajectory. The phase encoding direction is left-right. Eight loop coils are used in the simulation with coil sensitivity derived from the Biot-Savart law for circular loop coils. Complex Gaussian noise is added to the simulated data of all coils with zero mean and standard deviation that is 0.001 times the root-mean square value of all signals in the eight coils.

We used a simple a supervised neural network with 32 hidden layers. By applying above mentioned algorithm, in the training phase, the input data are the acquired data form the array of coils, where every non Cartesian point, per coil, will be paired separately by the nearest surrounding 5 non Cartesian points within the same coil and other coils in the array of coils according to the minimum Euclidian distance between points, and the output will be it is pair point, so the NN will be trained to optimize the weights needed for this shift, we use 1000 iteration for optimizing the weights and NN performance.

After the training phase reach optimum performance the trained NN will be used for the reconstruction phase, the Cartesian point will be estimated using the non Cartesian acquired data per each coil and relevant data within the other coils.

Here there are two strategies for reconstruction that can be used either using the nearest non-Cartesian data point to be shifted to the Cartesian point or the 4 surrounding non-Cartesian points will be used to estimate the Cartesian one.

The described reconstruction is applied to a real MR phantom acquired with a gradient echo sequence on a SIEMENS Trio system. With an array coil of eight channels using a spiral trajectory with 16 interleaves and 256 samples per leaf.

5.6. Results

Fig. 5.4 shows the results of applying the new method to the simulated SL data, where every coil has been reconstructed separately with a spiral trajectory. Fig. 5.5 shows the difference between the final SOS image for the coil array using the Neural network with the nearest non-Cartesian point strategy and the final SOS image for reconstructed SOS images the GROG algorithm. The Neural Network shows more homogeneous image quality with fewer artifacts in the main FOV. The results of applying the proposed method to the real MR phantom are shown in Fig. 5.6. The separated coil reconstruction. While Fig. 5.7 shows the SOS final image constructed using Neural Network for the real phantom data with the spiral trajectory using two different strategies for reconstruction and estimation of Cartesian points, one with the nearest non-Cartesian point and the other using the surrounding 4 non-Cartesian points.

In spite expectations to have more image quality using the 4 non Cartesian points as the Cartesian point will be estimated from more than one non Cartesian one , the nearest non Cartesian point show more image quality on the final image reconstruction with less

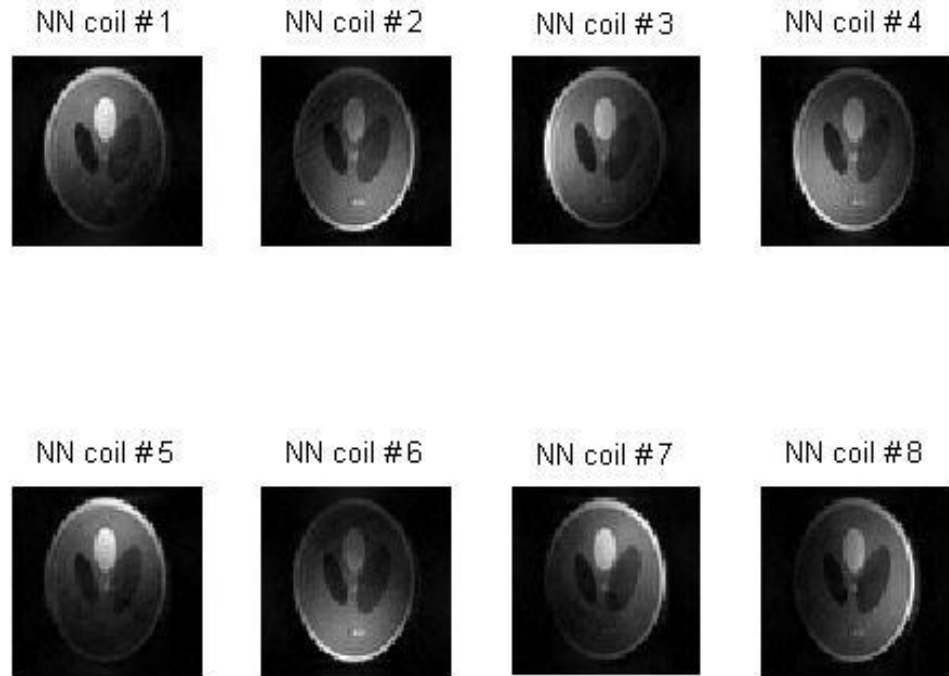


Figure 5.4. Show the reconstructed images for the eight coils of SL phantom with as spiral trajectory of width 128 using the Neural Network

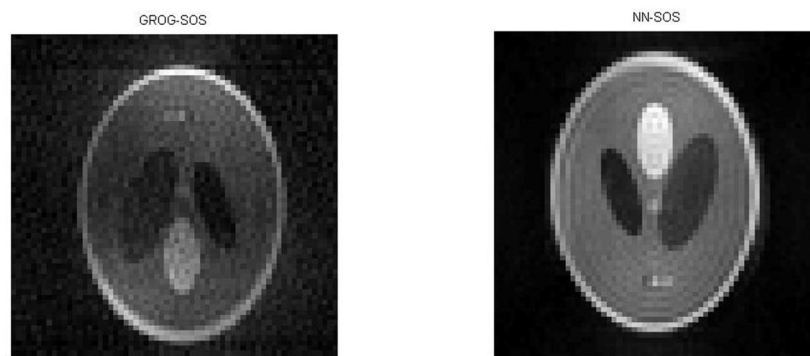


Figure 5.5 the reconstructed SOS images of GROG and Neural Network for Spiral Trajectory

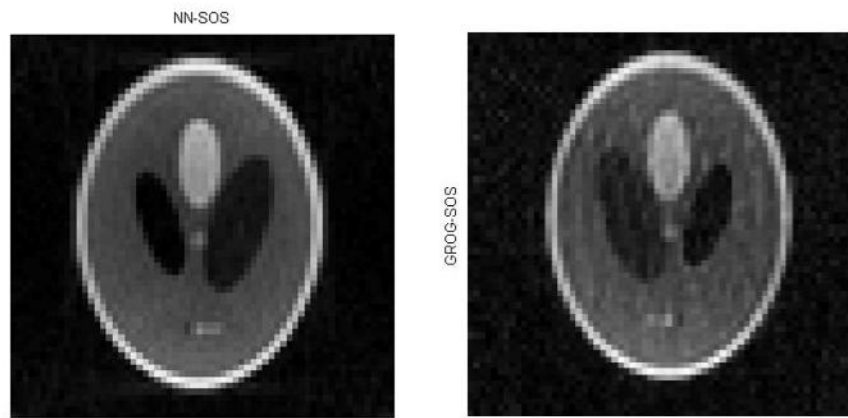


Figure 5.6 the reconstructed SOS images of GROG and Neural Network for radial Trajectory

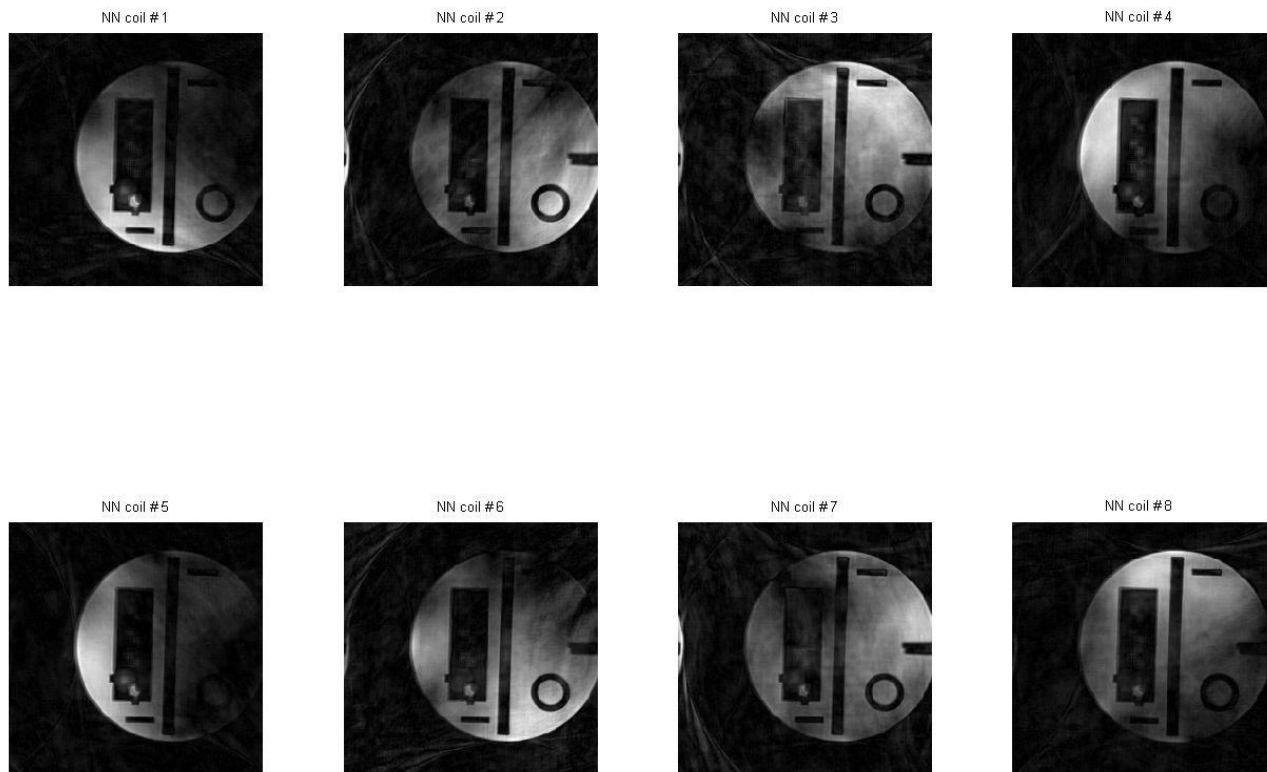


Figure 5.7. The reconstructed images for the real phantom data of eight coils with a spiral trajectory

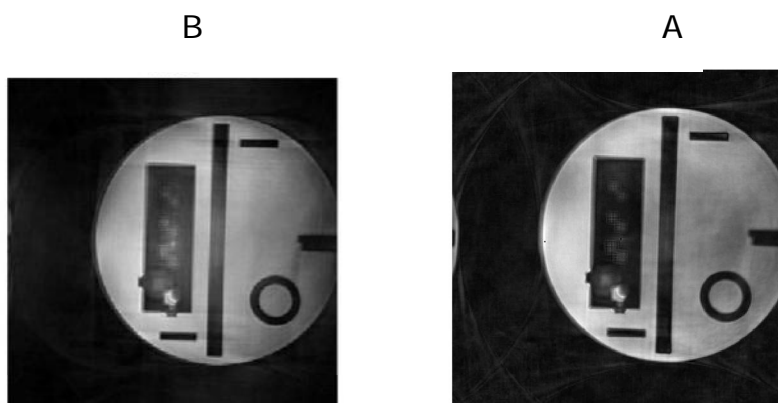


Figure 5.8. The reconstructed images of real phantom data using the nearest non Cartesian point strategy Fig .8.B, and using the surrounding 4 non Cartesian points to estimate the Cartesian point Fig 5.8.A

5.7. Discussion

The usage of NN in gridding the non Cartesian data has been demonstrated for radial, spiral trajectories. One advantage of NN, as well as GROG technique for gridding, is that no pre-calculated DCFs or other parameters are required for gridding, whereas convolution gridding requires a DCF in addition to other parameters. While this is not a difficulty for the radial or spiral trajectory, the ability to grid BLADE, rosette, or stochastic data without having to calculate a DCF is highly advantageous[21,22,23,24].

There are other methods besides NN and GROG techniques that perform data gridding without the need for a DCF. For instance, Uniform Resampling/Block Uniform Re-sampling (BURS) [24] is a method that performs data re-sampling by transforming the gridding problem into a linear equation which can be solved using singular value decomposition (SVD). As in NN and GROG, no sub-sampling is employed for the gridding process and no DCF is required. However, this family of methods has several drawbacks. In the URS method, the large number of data samples leads to an inconveniently large linear equation. The BURS method is somewhat more practical, although it is highly sensitive to noise due to the need for a matrix inversion in the SVD.

The extension to these approaches, regularized block uniform resampling (rBURS) [24] , addresses this noise sensitivity problem, although the results are strongly dependent on the parameterization of the matrix inversion problem, i.e., the regularization and the size of the region of support.

However, the main advantages for the NN technique over other techniques like GROG is the no need for oversampling the acquired data per each coil over the read out direction, which was an essential step specially for the datasets with the low SNR. As the SNR loss can be attributed to the application of weight sets to the individual noisy pints, which amplifies the noise into the shifted point. The application of NN to simulated data and real phantom data as on fig 5.5, fig5.5 and fig 5.8 respectively show a good image quality for the final SOS image as well as coil images without need for oversampling the data.

The other difference between the application of NN and GROG technique is the no need for a pre-calibration data set, to get the base weight, or pre-requisite need for special trajectory with Cartesian sampling to be inherited. As shown in fig.5.5 the usage of NN can be applied to simulated phantom with a spiral trajectory, without any pre-calibration

Data the final SOS image show an improvement image quality over the GROG with a pre-calibration data. Fig 5.8 show also a good image quality with using of NN for real phantom data with a spiral trajectory without need for a pre-calibration data and with two different reconstruction criteria.

However, instead of above mentioned advantages for the NN technique the final SOS image show a some artifact, an expected source of the artefact is due to using a real-valued NN instead of complex-valued NN. Treating real and imaginary parts separately may be the trained weights for each part vary independently causing the ghosting artifact as we see in NN-images. This is known as quadrature-ghost, and it may be expected, these artifact can be reduced by using a complex-valued NN.

In spite the great performance of the NN in gridding, the NN architecture itself may be need a more focus in order to optimize the NN components like the number of hidden layers, Activation function, this optimization may either increase the performance of the NN lead to good performance in the reconstructed image or decrease the training and reconstruction time for the NN.

5.8. Conclusion

The NN proposed technique here is an alternative and improvement step over the current methods for the gridding of non-Cartesian datasets. Instead of employing a convolution window as in the gold-standard gridding, the NN is instead used to be trained to shift the non-Cartesian data points to their nearest Cartesian locations without need for oversampling the acquired data as well as the need for a pre-calibration data sets which enable the N technique to be used with many non uniform trajectories.

The NN show a good potential to be used as pre step with the parallel imaging for non Cartesian data set as it can the under sampled non-Cartesian datasets to yield Cartesian data points near the sampled locations and zeros in all other locations could even be advantageous for other types of non-Cartesian parallel imaging reconstructions.

The need for using a complex valued NN with optimised architecture is considered a potential point for future work, with the those way of modifications we can decrease the presence artefacts in the final reconstructed image in spite the good and diagnostic image quality of the reconstructed image, however the scope of using NN in this work was as a tool to overcome current limitations in the current technique.

Chapter 6

Conclusions and Future Work

In this chapter the contributions made by this dissertation are summarized, and possible future extensions and applications are discussed.

6.1 Uniform Sensitivity

The new method for parallel imaging acquisition and reconstruction that improves the current GRAPPA technique in terms of image uniformity over the entire FOV by using simultaneous acquisition between body coil and local surface coil proposed in this dissertation is a promising method to improve the final reconstructed image, as this image is sum of square image from the array of surface coils so, no phase information will be presented in the image. So, the new method can add a uniform sensitivity by using the phase information from the body coil which is uniform over the field of view. Moreover, this new technique can be extended to be combined with other parallel imaging, as Auto-sense, by overcoming the current hardware limitations for this technique to acquire the data simultaneously between the body coil and local array coil this technique can improve the phase information for the final image reconstruction. The reduction of the

noise accompanied with the body coil data considered a potential point for more work as it will improve and decrease the apparent artefacts into the final reconstructed image.

6.2 Variable Block GRAPPA

We proposed a variable-size convolution kernel instead of the fixed-size kernel initially employed in GRAPPA. The variable-size kernel follows directly from the mutual coil sensitivity of each coil pair. The kernel is defined through the ratio of the sensitivities of each pair of coils which depends on the inherent sensitivity of each coil and the geometry of the coil array. The kernel is a 2D function and is concentrated in a direction

That depends on the location of the two coils under consideration relative to each other. The proposed approach of using variable-size kernel can improve our understanding of how GRAPPA works and can help in optimizing the reconstruction as well as the selection of various scan parameters like the number and locations of the ACS lines.

6.3 Using the Neural Network to solve the gridding problem

We proposed a new technique to solve the gridding problem associated with the non uniform sampling by employing The Neural Network as an alternative and improvement step over the current methods for solving the gridding. Instead of employing a convolution window as in the gold-standard gridding, the NN is instead used to be trained

to shift the non-Cartesian data points to their nearest Cartesian locations without need for oversampling the acquired data as well as the need for a pre-calibration data sets which enable the N technique to be used with many non uniform trajectories.

Some potential points can be expected as future work i.e., the Neural Network architecture itself may be need a more focus in order to optimize the Neural Network components like number of hidden layers, Activation function and the usage of complex Neural Network, this optimization may increase the performance of the Neural Network or decrease the training and reconstruction time for the Neural Network.

REFERENCES

- [1] Ray H. Hashemi, and William G. Bradley, "MRI: the basics," Williams & Wilkins, 1997.
- [2] Y.M. Kadah, K. Heberlein, and X. Hu, "Floating navigator echo for in-plane translational motion estimation," *ISMRM 10 th Scientific Meeting*, Honolulu, p. 2309, May 2002.
- [3] King KF, Zhou XJ, "Handbook of MRI sequences." Elsevier Academic Press, London, pp 546–557.
- [4] Margosian P, Schmitt F, Purdy D." Faster MR imaging: Imaging with half the data". *Health Care Instrumentation* 1: 195–197.
- [5] Xu Y, Haacke EM. "Partial Fourier imaging in multidimensions: a means to save a full factor of two in time." *Journal of Magnetic Resonance* 14: 628–635
- [6] A. Sodickson, "Breaking the magnetic resonance speed barrier: Implications of parallel imaging," www.appliedradiology.com, Accessed: April, 2005.
- [7] M. Blaimer, F. Breuer, M. Nittka, R. Heidemann, Griswold M., et al., "SMASH, SENSE, PILS, GRAPPA: How to choose the optimal method," *Topics in Mag. Res. Med*, vol. 15, pp. 223–236, August 2004.
- [8] K. Pruesmann, M. Weiger, M. Scheidegger and P. Boesiger, "SENSE: Sensitivity encoding for fast MRI," *Mag. Res. Med*, vol. 42, pp. 952–962, November 1999.
- [9] M. Griswold, P. Jakob, M. Nittka, J. Goldfarb and A. Haase, "Partially parallel imaging with localized sensitivities (PILS)," *Mag. Res. Med*, vol. 47, pp. 602–609, October 2000.

- [10] D. Sodickson and W. Manning, "Simultaneous acquisition of spatial harmonics (SMASH): Fast imaging with radiofrequency coil arrays," *Mag. Res. Med.*, vol. 38, pp. 591–603, July 1997.
- [11] P. Jakob, M. Grisowld, R. Edelmann and D. Sodickson, "AUTO-SMASH: A self-calibrating technique for SMASH imaging," *Magnetic Resonance Materials in Physics, Biology and Medicine*, vol. 7, pp. 42–54, November 1998.
- [12] R. Heidemann, M. Griswold, A. Haase and P. Jakob, "VD-AUTO-SMASH imaging", *Mag. Res. Med.*, vol. 45, pp. 1066–1074, December 2001.
- [13] M. Griswold, P. Jakob, R. Heidemann, M. Nittka, V. Jellus, et al., "Generalized auto-calibrating partially parallel acquisitions (GRAPPA)," *Mag. Res. Med.*, vol. 47, pp. 1202–1210, June 2002.
- [14] W. Kyriakos, L. Panych, D. Kacher, CF. Westin, S. Bao, et al., "Sensitivity profiles from an array of coils for encoding and reconstruction in parallel." *Mag. Res. Med.*, vol. 44, pp. 301–308, February 2000.
- [15] FH. Lin, K. Kwong, J. Belliveau and L. Wald , "Parallel imaging reconstruction using automatic regularization," *Mag. Res. Med.*, vol. 51, pp. 559–567, March 2004.
- [16] L.A. Shepp and B.F. Logan, "Reconstructing interior head tissue from X-ray transmission," *IEEE Trans. Nucl. Sci.* NS-21, pp. 228-236, 1974.
- [17] M. A. Bernstein, K. F. King and X. J. Zhou, "Handbook of MRI Pulse Sequences," Elsevier Science & Technology Books, 2004

- [18] N. F. Osman , S. Sampath , E. Atalar and J. L. Prince, “Imaging longitudinal cardiac strain on short-axis images using strain-encoded MRI,” *Mag. Res. Med* ,vol. 46, pp. 324 - 334, 24 Jul 2001
- [19] Yufang Bao; Maudsley, A.A. “Image reconstruction in the GRAPPA algorithm formalism”. 4th *IEEE International Symposium on Biomedical Imaging*, Vol , 12-15 pp.113 – 116,2007.
- [20] Meyer CH, Hu BS, Nishimura DG, Macovski A. “Fast spiral coronary artery imaging.” *Mag. Res. Med*, 1992;28: 202–213
- [21] Jackson JI, Meyer CH, Nishimura DG, Macovski A. “Selection of a convolution function for Fourier inversion using gridding.” *IEEE Trans Med Imaging* 1991; 10:473 478.
- [22] Pipe JG. “Motion-correction with PROPELLER MRI: application to head motion and free-breathing cardiac imaging”. *Mag. Res. Med* 1999; 42: 963–969.
- [23] Noll, DC. “Multishot rosette trajectories for spectrally selective MR imaging”. *IEEE Trans Med Imaging* 1997;16:372–377.
- [24] Rosenfeld D. “New approach to gridding using regularization and estimation theory”. *Mag. Res. Med* 2002;48:193–202.
- [25] Moriguchi H, Duerk JL. “Iterative next-neighbor regridding (INNG): improved reconstruction from nonuniformly sampled k-space data using rescaled matrices”. *Mag. Res. Med* 2004; 51:343–352.

[26] Gabr RE, Aksit P, Bottomley PA, Youssef AB, Kadah YM. “Deconvolution-interpolation gridding (DING): accurate reconstruction for arbitrary k-space trajectories”. *Mag. Res. Med* 2006; 56:1182–1191.

[27] Seiberlich N, Breuer FA, Blaimer M, Barkauskas K, Jakob PM, Griswold MA. “Non-Cartesian data reconstruction using GRAPPA operator gridding (GROG)”. *Magn Reson Med* 2007; 58:1257–1265.

[28] N.Seiberlich,1 Felix Breuer, Martin Blaimer, Peter Jakob and Mark Griswold, “Self-Calibrating GRAPPA Operator Gridding for Radial and Spiral Trajectories”. *Mag. Res. Med, 2008; 59: 930-935.*